NASA
SATELLITE COMMUNICATIONS APPLICATION RESEARCH
PHASE II FINAL REPORT

EFFICIENT HIGH POWER, SOLID STATE AMPLIFIER FOR EHF COMMUNICATIONS

31 July 1993

Period of Performance:

June 9, 1992 to July 31, 1993

Rockwell International
Tactical Systems Division
3370 Miraloma Street
Anaheim, CA 92803-4921

NASA
SATELLITE COMMUNICATIONS APPLICATION RESEARCH
PHASE II FINAL REPORT

EFFICIENT HIGH POWER, SOLID STATE AMPLIFIER FOR EHF COMMUNICATIONS

31 July 1993

Contract Number NASW-4513

Period of Performance:
June 9, 1992 to July 31, 1993

Submitted To:

National Aeronautics and Space
Administration Headquarters

Space Research Division
(Code RSR)
Washington, DC 20546

James Benet, Principal Investigator

Rockwell International
Tactical Systems Division
3370 Miraloma Street
Anaheim, CA 92803-4921

TABLE OF CONTENTS

ILLUSTRATIONS

LIST OF TABLES

NASA SATELLITE COMMUNICATIONS APPLICATION RESEARCH (SCAR)

PHASE II FINAL REPORT

1.0 SCOPE

This final report describes the work performed from June 9, 1992 to July 31, 1993 on the NASA Satellite Communications Application Research (SCAR) Phase II program, "Efficient High Power, Solid State Amplifier for EHF Communications." The contract number is NASW-4513.

2.0 INTRODUCTION

2.1 Background

Advanced satellite communication systems (such as ACTS and MILSTAR) use Extremely High Frequency (EHF) bands (millimeter-wave) to achieve wide channel bandwidths. An optimum means of obtaining high power (RF) signal levels for transmitting data in these EHF bands has not been obtained. The problem is also applicable to airborne EHF radar systems.

Traveling wave tube (TWT) amplifiers produce sufficient output power (10 to 300 watts) in these bands; however, there are several problems associated with tube technology which impact costs. These include size, weight, reliability, catastrophic failure, and producibility. Many of these problems are associated with the kilovolt power supplies needed to power the tubes.

Solid state Impatt diode amplifiers do not require kilovolt power supplies; however, these devices have only limited output power, small gain (typically, 3 to 6 dB), and low efficiency (typically, less than 10%). In addition, they inject a substantial amount of noise into the transmitted signal. Circulators (which increase size, weight, and costs) are needed to maintain stability with these two-terminal devices. Cavity-combined Impatt amplifiers are limited to about 8-way combining levels which is not always sufficient for certain system applications. Corporate-combined Impatt amplifiers become large and inefficient due to the size of the corporate combiner.

In contrast to Impatt amplifiers, three-terminal, solid state transistor amplifiers provide higher gain, unconditional stability, and higher efficiency; however, their output power is lower. For a good EHF power transistor, the frequency-power product is typically under 6 GHz-watts, the typical gain-fre-

quency product is 400 GHz, and the power added efficiency ranges between 10 and 30 percent. In addition, these devices offer lower noise figures and better reliability characteristics than either the Impatt or the TWT. The major problem is insufficient output power.

Typical means of combining output power from several transistor amplifiers using corporate, radial, or two-dimensional spatial combiners have severe limitations. The combining loss of microstrip corporate combiners becomes high for summing more than 16 amplifiers due to the current losses in the microstrip lines as the structure becomes large. Size is also a problem with waveguide corporate combiners. Circumferential resonant moding is a problem with large waveguide radial combiners for combining levels over 30.

Two-dimensional spatial combining provides a means to efficiently combine output power from large numbers (50 to 500) of solid state transistor amplifiers. Combining losses are minimized (typically 1 dB) because combining is done spatially (in parallel) in a near-lossless medium. Unlike corporate combiners, losses are virtually independent of the number of elements being combined.

Two-dimensional, spatial power combiners have not been widely used due to several problems associated with feedthrough spatial combiners, for example: (1) Heat generated by the array of amplifiers cannot be readily dissipated, (2) Fabrication and installation are difficult, complex, and costly, and (3) Routing RF signal to the back side of the array (where the combiner horn is located) requires bonding RF interconnections which degrade reliability and performance at EHF.

The goal of this research is to demonstrate the feasibility of high efficiency, high power, EHF solid state amplifiers which are smaller, lighter, more efficient, and less costly than existing traveling wave tube (TWT) amplifiers. The new concept uses a unique orthomode spatial power combiner (OSPC) with monolithic microwave integrated circuit (MMIC) technology to resolve the issues mentioned above.

2.2 Technical Concept

The OSPC uses the principle of orthogonally polarized electromagnetic waves to isolate signals going into and out of a planar array of amplifiers. Its operation is illustrated in the schematic diagram shown in Figure 1 and in the conceptual layout shown in Figure 2. A tapered horn is used to direct vertically-polarized fields to a planar array of amplifiers.

Orthogonally polarized radiating elements on the array receive a vertically polarized wave and convert it to quasi-transverse electromagnetic (TEM) fields on microstrip lines on the array board. The signals are amplified and sent to the horizontally polarized port of the radiating element. The signals are re-transmitted back through the horn using horizontal polarization. An orthomode transducer on the throat of the horn separates and isolates the two orthogonal (vertically-polarized input and horizontally-polarized output) signals. Since the radio frequency (RF) energy enters and leaves the array on the same side, the back side of the array can be used for heat sinking and biasing. This approach makes the OSPC amplifier fully compatible with full-scale, monolithic microwave integrated circuit (MMIC) wafer integration. The array can be formed from one or more gallium arsenide (GaAs) MMIC wafers.

Since combining efficiency of spatial power combiners is virtually independent of the number of elements being combined, several hundred low-to-medium power EHF solid state amplifiers can be combined to produce high-efficiency, high-power solid state amplifiers at EHF bands.

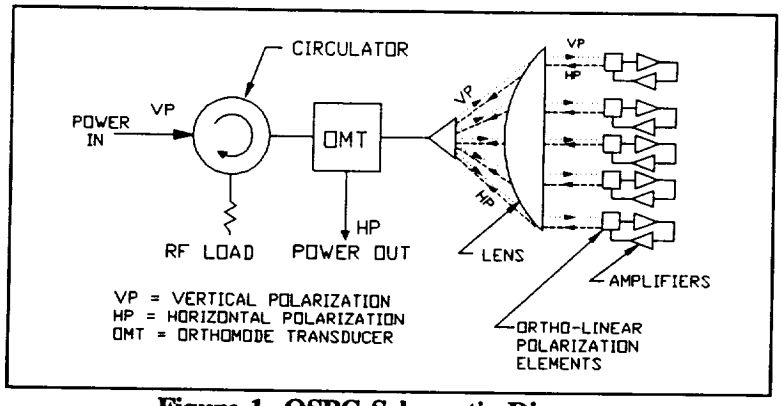

Figure 1 OSPC Schematic Diagram

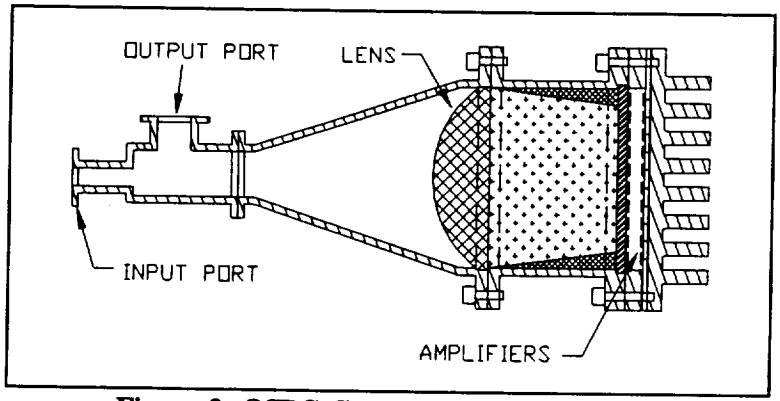

Figure 2 OSPC Conceptual Configuration

2.3 Program Objectives

The purpose of this program was to demonstrate the feasibility of high-efficiency, high-power, EHF solid state amplifiers that are smaller, lighter, more efficient, and less costly than existing traveling wave tube (TWT) amplifiers by combining the output power from up to several hundred solid state amplifiers using a unique orthomode spatial power combiner (OSPC). The program was divided into two phases.

2.3.1 Phase I Objectives

The specific objective of the Phase I program was to verify conceptual feasibility of a passive OSPC by designing, fabricating, and testing a proof-of-concept model at 17 GHz to achieve the performance goals listed in Table 1.

Table 1
Design Goals for the Phase I Passive OSPC

Parameter	Goal
Bandwidth	> 13%
20 dB Isolation	> 20 dB
Insertion Loss (2-way)	< 3 dB
VSWR	< 2:1

2.3.2 Phase II Objectives

The specific objective for Phase II was to verify conceptual feasibility of achieving power gain with an **active** OSPC amplifier by designing, fabricating, and testing a proof-of-concept amplifier model operating at Ku-band. The technical goal was to achieve over 5 watts output power by spatially combining power from a planar array of 69 monolithic microwave integrated circuit (MMIC) amplifier elements each having output power of 100 milliwatts. The horn structure was to be optimized for field uniformity during Phase II of the program. The specific design goals for the 17-GHz OSPC amplifier are shown in Table 2.

Table 2 Design Goals for the Phase II OSPC Amplifier

Parameter	Goal
Bandwidth	≥ 10%
RF Amplifier Gain	≥ 10 dB
Number of Elements	= 69
Total Power Output	≥ 5 Watts
Input/Output VSWR	< 2:1

3.0 SUMMARY OF ACCOMPLISHMENTS

The following two sections summarize the results and accomplishments of the program during Phase I and Phase II. Phase I results are more fully described in the Phase I interim status and final reports, references [1] through [3]. Interim status reports (references [4] through [6]) were also written during Phase II. Detailed results of the Phase II program are contained in Section 4.

3.1 Phase I Program Accomplishments

In Phase I the high efficiency performance of a passive OSPC was demonstrated by building a proof-of-concept model and by performing measurements to determine its efficiency. The OSPC was designed, built, and tested for operation at 17 GHz. It combined the output signals from a 69-element passive array.

Uniform field distribution across the aperture of the array is necessary to obtain maximum output power and efficiency from a spatially combined array of amplifiers. In a design trade-off study conducted early in the Phase I program, it was shown that a spatially-combined amplifier driven with a cosine or J_o-Bessel E-field distribution would provide only 33% of the output power and 66% of the efficiency than can be obtained using a uniform E-field distribution.

Scharten, et. al. [7] achieved uniform field distribution by placing longitudinal slots in a conical feedhorn. In another paper, Aly and Mahmoud [8] showed that loading the slots with a dielectric decreases the slot depth while increasing the polarization isolation.

Figure 3 shows the cross-sectional view of the Phase I conical horn with a longitudinal slotted section. In this design the fins that form the slots are extended four inches back from the mouth of the horn. Half the length of the fins are tapered to provide a smooth transition. The section has ninety slots around a 4.6-inch diameter inside aperture. The 0.456-inch deep slots are filled with dielectric foam having a relative dielectric constant of 1.12.

A three-piece dielectric lens at the horn aperture is used to correct for the spherical phase front. The center section is flat on one side and has a hyperbolic curvature on the other side. The lens is 0.441 inch thick at the center. The relative dielectric constant is 2.54. The two outer lens pieces have a relative dielectric constant of 1.7 and serve as quarter-wavelength impedance matching sections.

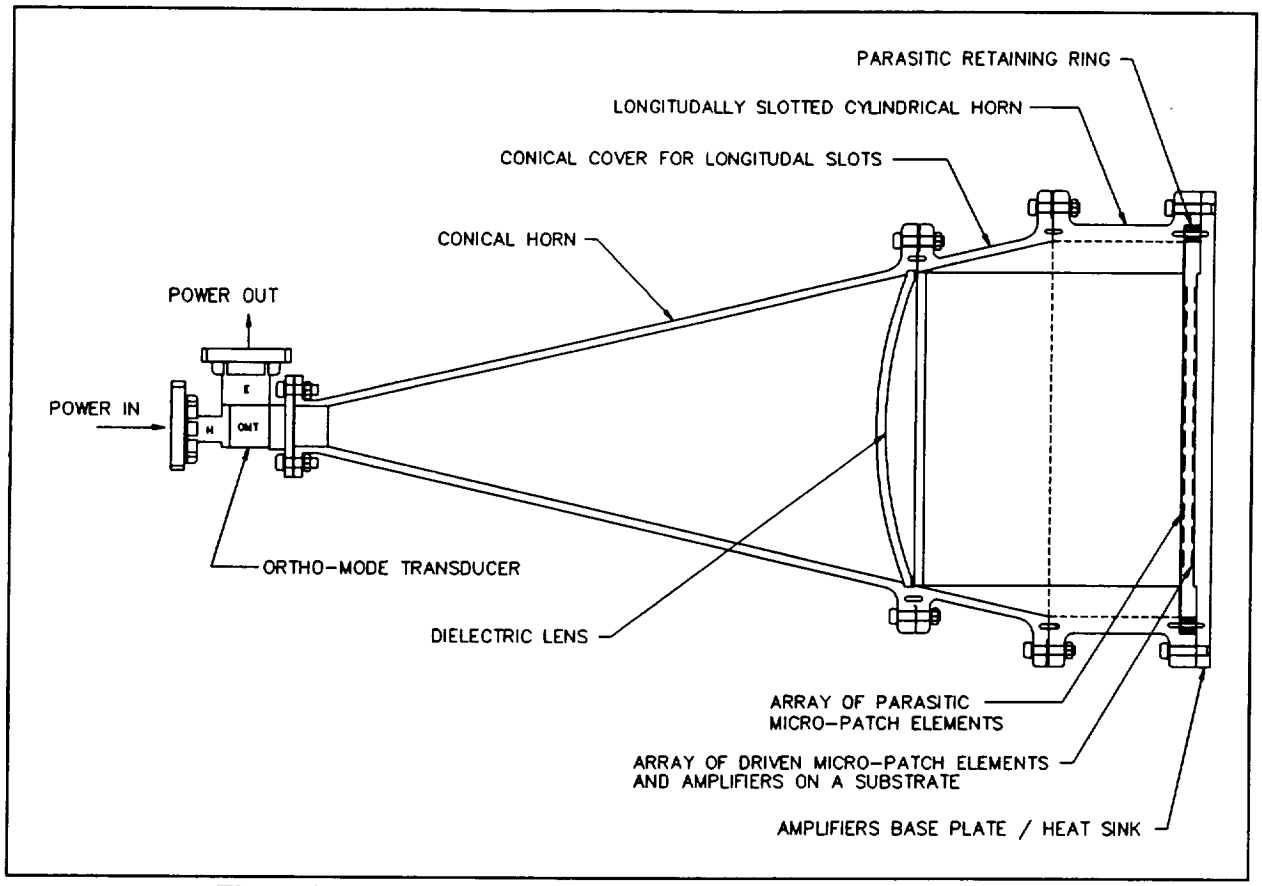

Figure 3 Cross-sectional view of the Phase I conical horn design

The conical horn combiner was first tested with a passive micropatch array. Figure 4 shows the measured 2-way transmission loss of the conical horn along with the input return loss. The response shows peaks of less than 2.5 dB which includes 0.6 dB of microstrip transmission line loss on the array board. When this loss is subtracted from the response loss, the one-way combining loss is determined to be about 1.0 dB (or 80% efficiency). The return loss was greater than 10 dB and the polarization isolation was greater than 20 dB.

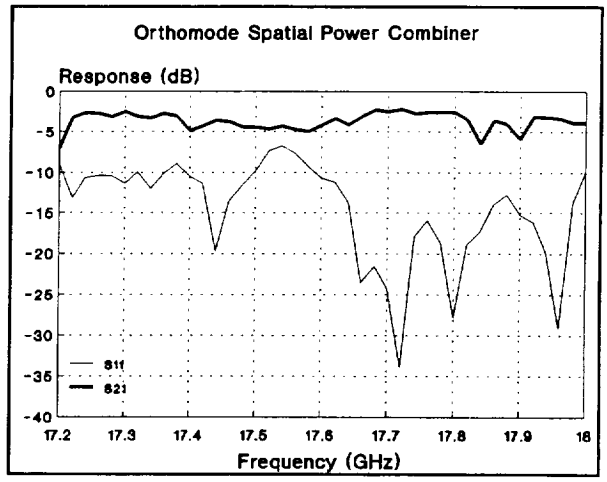

Figure 4 Measured two-way response of Phase I spatial power combiner

The conical horn combiner was then tested for uniform fields. Far-field radiation patterns of the conical horn were measured without the array boards. These patterns matched those of a horn with a TE_{11}-mode field distribution. The expected uniform field distribution was not achieved because the fields were not set up properly in the slotted section of the horn. Conversion of TE_{11}-mode field distribution to uniform field distribution should be initiated near the throat of the horn where the aperture is small enough to support only the dominant uniform mode. As a result, the conical horn exhibited higher-order mode propagation .

3.2 Phase II Program Accomplishments

In Phase II, trade-off design studies were undertaken and a new horn structure was designed along with a prototype amplifier circuit. The new horn differed from the Phase I longitudinally slotted horn in that the slots were extended all the way back to the throat of the horn. The horn structure was fabricated and then tested on the network analyzer. The peak 2-way transmission loss was 5.0 dB. This was 2.5 dB greater than the Phase I horn. The higher loss was attributed to the higher loss tangent of the dielectric foam material in the slots (tan δ=0.008) and to the extension of the slots to the throat of the horn. The peak return loss ranged from 10 to 15 dB. Far-field pattern measurements were taken on the new longitudinally slotted horn at 16, 17, and 18 GHz. The patterns indicated that the horn produced near-uniform field distribution.

The prototype amplifier circuit was fabricated and tested for gain and return loss. The transmission gain of the initial circuit was 10 dB and its minimum return loss was 10 dB in the forward direction and 5 dB in the reverse direction. The amplifier was then tuned for improved impedance match. The tuning improved the output match to obtain 15-dB return loss. The amplifier circuit was characterized for RF output power as a function of input power and bias voltage. The amplifier circuit layout was then incorporated into array pattern.

The array was fabricated and assembled with the amplifier elements. Output power from each amplifier element was observed on a spectrum analyzer to confirm the operation of each amplifier element. The array was then assembled into the OSPC combiner horn and biased on. Observations from the output of the horn on a spectrum analyzer revealed that the OSPC amplifier oscillated at 16.4 GHz when biased to produce more than 3 dB gain (with the Phase I horn). The oscillation were attributed to higher-order mode resonances within the feedhorn. To simulate a space-fed condition a second test was performed without any enclosing horn structure except the last (interface) section of the

Phase II combiner. No oscillations were observed on the spectrum analyzer even when RF power was injected into the input port of the orthomode transducer. The amplitude of the output signal increased as the bias voltage to the array was increased from 2.0 to 8.5 volts. The 8.5-volt bias corresponds to maximum gain of 12 dB for each amplifier. This indicated that the active amplifier array produced gain.

A biasing mishap occurred when tests were performed on the network analyzer. Before the response from the space-fed horn on the network analyzer display could be recorded, the devices in the array burned out.

The test results observed indicate that an OSPC amplifier designed with space-fed horn has the potential function as a spatially-combined power amplifier. The observations helped to identify design problems and to generate solutions to improve the OSPC amplifier to achieve high-efficiency, for application as a solid state amplifier for millimeter-wave applications.

Two design improvements to eliminate oscillations in the OSPC amplifier were identified and examined as a result of this program: (1) A new space-fed feedhorn that eliminates higher-order mode resonances in the feedhorn while providing uniform field distribution and (2) A new array circuit layout which reduces undesirable radiation and coupling of the microstrip lines which interface the amplifier circuit to the patch radiating elements in the array. A preliminary design and performance analysis was performed on the new space-fed feedhorn. The analysis showed that the new design has the potential to enable the OSPC amplifier to achieve its intended design goals.

4.0 PHASE II TECHNICAL ACCOMPLISHMENTS

The following tasks were completed on the Phase II NASA SCAR program: (1) a new OSPC horn was designed, fabricated, and tested; (2) a prototype amplifier circuit was designed, built, and characterized; (3) the amplifier array was fabricated and its operation was confirmed; (4) the array was assembled in the OSPC and tested; and (5) a new space-fed lens feedhorn was designed and analyzed. Details of these accomplishments are presented in the following sections.

4.1 Phase II OSPC Horn

A new OSPC feedhorn was designed with the length of the slots extended back to the throat of the horn to couple more power into the slots. A cross-sectional view of the entire OSPC amplifier assembly is shown in Figure 5. The horn was fabricated from aluminum stock in four sections because this facilitated fabrication using wire electrical discharge machining (EDM). The sections (listed from throat to mouth) are as follows: (1) Aft transition, (2) Aft horn, (3) Forward horn, and (4) Forward transition. Table 3 shows the dimensions of each section.

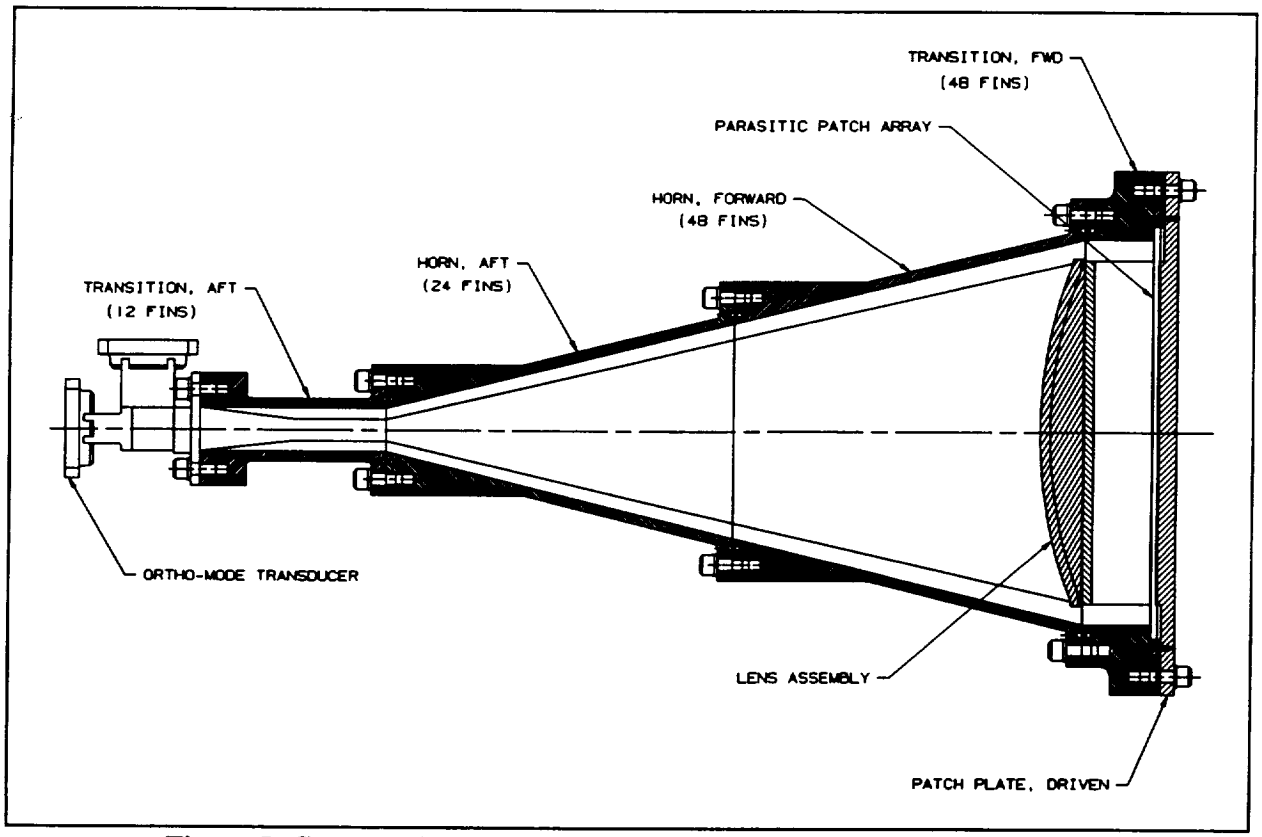

Figure 5 Cross-sectional view of the Phase II OSPC amplifier assembly.

After machining, the horn sections were zincated then nickel- and gold-plated. The thickness of the gold was 100 micro-inches. The sections were completely filled with a granular syntactic form (Emerson & Cumings Eccofoam EFF-14) and cured for 4 hours at 230 °F. The hardened foam on the

Table 3 Dimensions of the Phase II Horn Sections in Inches

Section	Length	# Slots	Input Side		Output Side	
			Aperture Diameter	Wall Diameter	Aperture Diameter	Wall Diameter
1) Aft Transition	2.500	12	0.590	0.590	0.300	0.590
2) Aft Horn	4.657	24	0.300	0.590	2.450	2.870
3) Forward Horn	4.657	48	2.450	2.870	4.600	5.150
4) Forward Transition	1.000	48	4.600	5.150	4.600	5.150

central region of each section was removed using a cutting tool on a lathe. The sections were then bolted together to form the horn. The 3-piece dielectric lens was inserted between the forward horn and the forward transition section before they were bolted together.

Photographs of the Phase II horn are shown on the next three pages. Figure 6 shows the profile of the horn. The dielectric foam material can be seen filling up the slot area between the fins. The white material inside the aperture of the horn is the output side of the last section of 3-piece dielectric lens. The patch arrays are shown in Figure 7. The parasitic patch array is shown mounted to the horn. The driven array is shown separately adjacent to the horn. The driven array shown in the photograph is a passive array; ie., it does not contain the active amplifier elements. The output from the vertically-polarized port of the patch element is connected (via a microstrip line) to the input of the horizontally-polarized port of the radiating element. This array was used for testing for combiner losses. Donut-shaped, metallic spacer rings (not shown in the photograph) fit around the flanges between the two arrays to adjust the spacing to obtain the best impedance match, thus, minimizing reflections. The photograph presented in Figure 8 shows the combiner in its completely assembled configuration with the passive driven array.

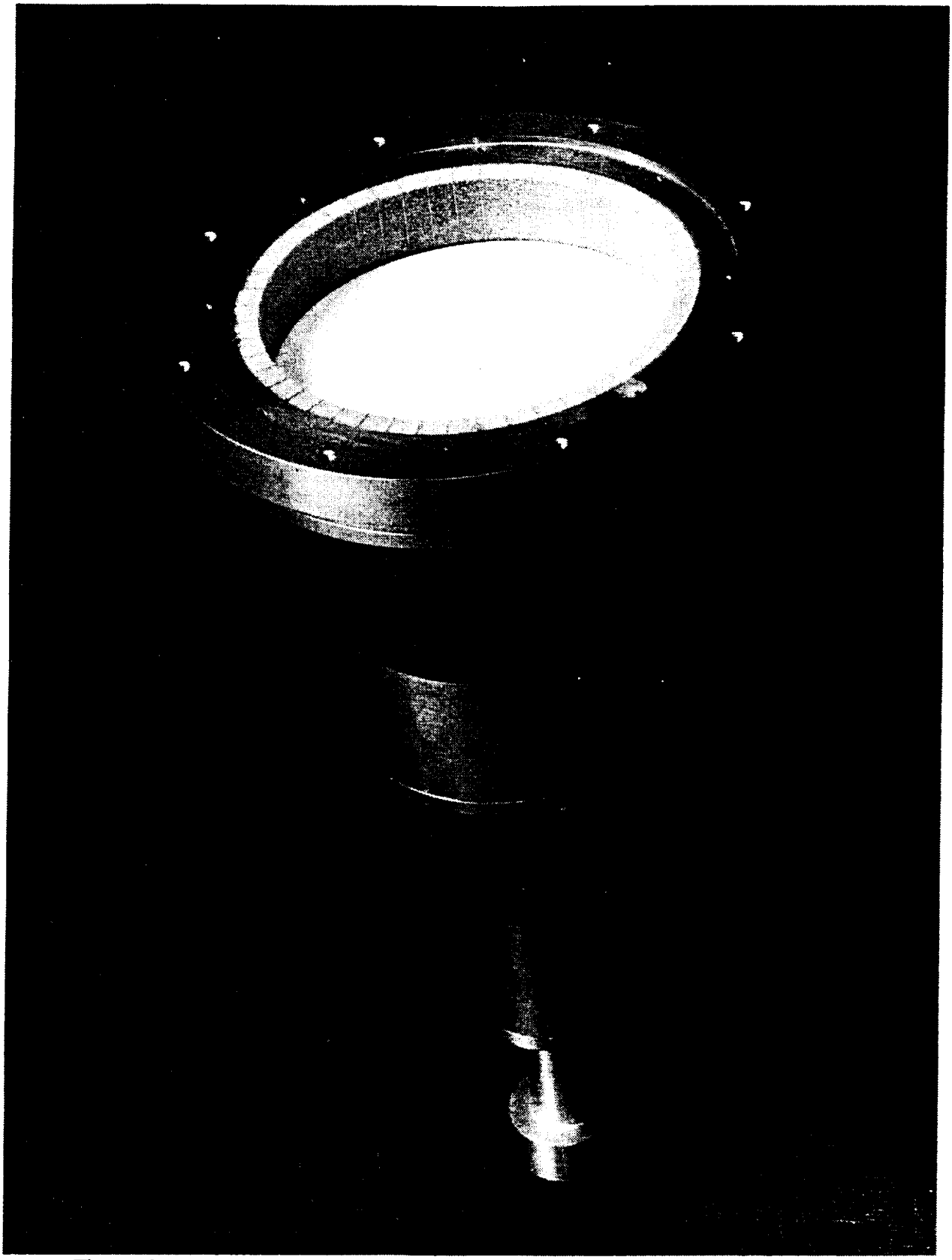

Figure 6 Photograph of profile view of the horn showing part of the dielectric lens

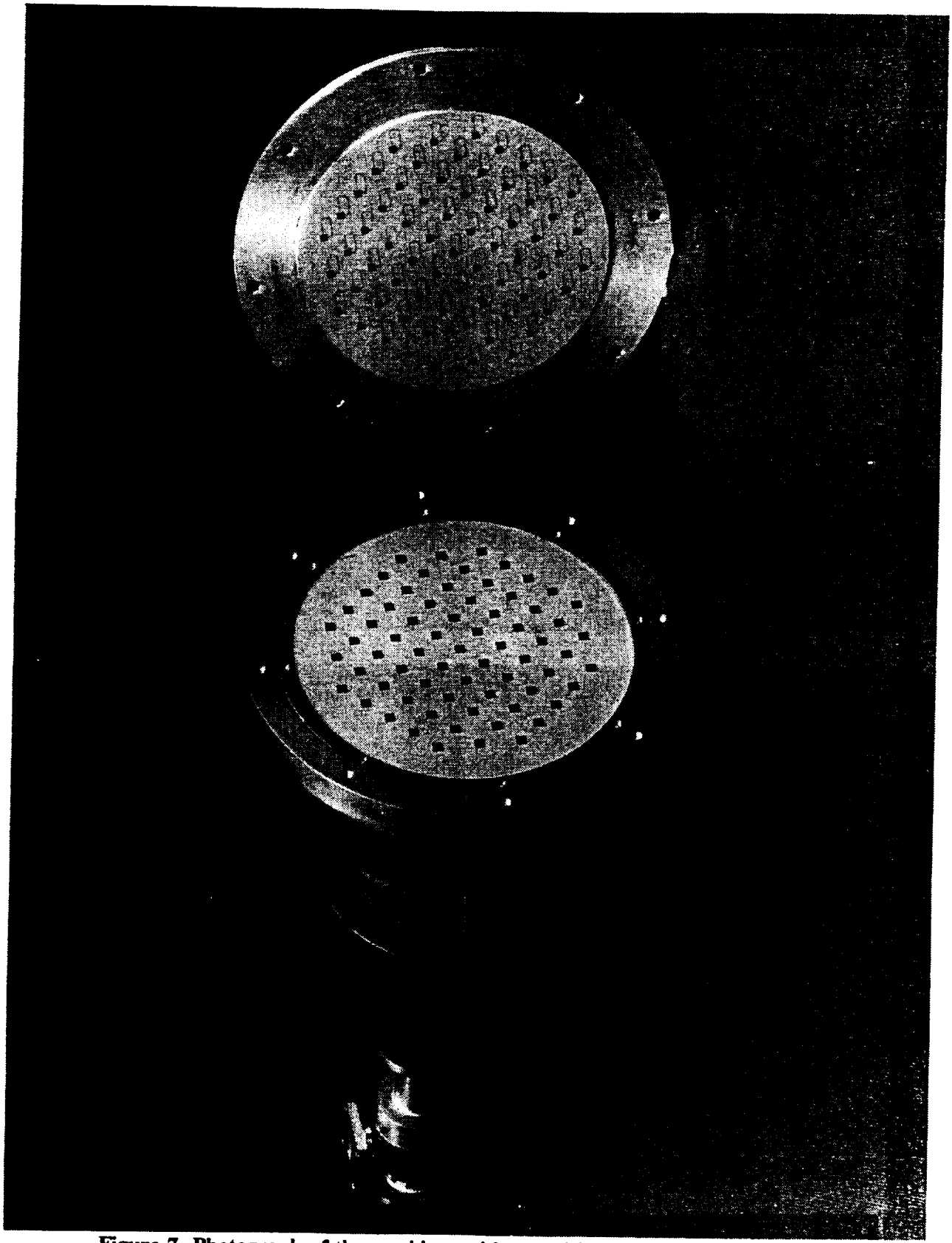

Figure 7 Photograph of the combiner with parasitic and driven patch arrays

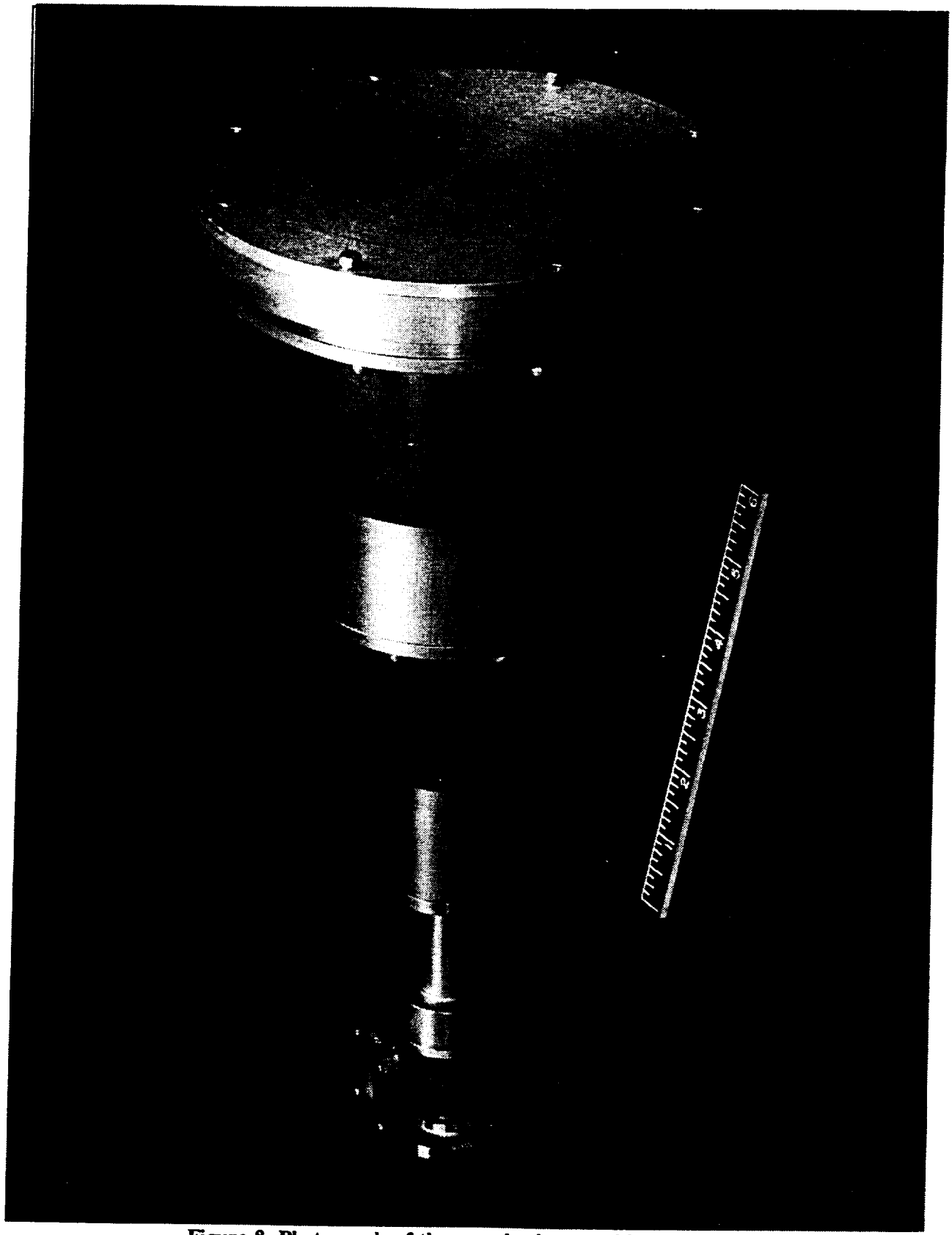

Figure 8 Photograph of the completely assembled combiner

The combiner shown in the previous photographs was assembled and tested for reflection and insertion loss using a Hewlett Packard 8510B automatic network analyzer. Reflection measurements of the open-end horn radiating into free space were first taken to show that the horn was properly designed to preclude high mismatches. A plot of the measurement data, which includes a small amount of mismatch from a coax-to-waveguide adapter, is shown in Figure 9. This data falls within the expected range for the horn (approximately 15 dB return loss).

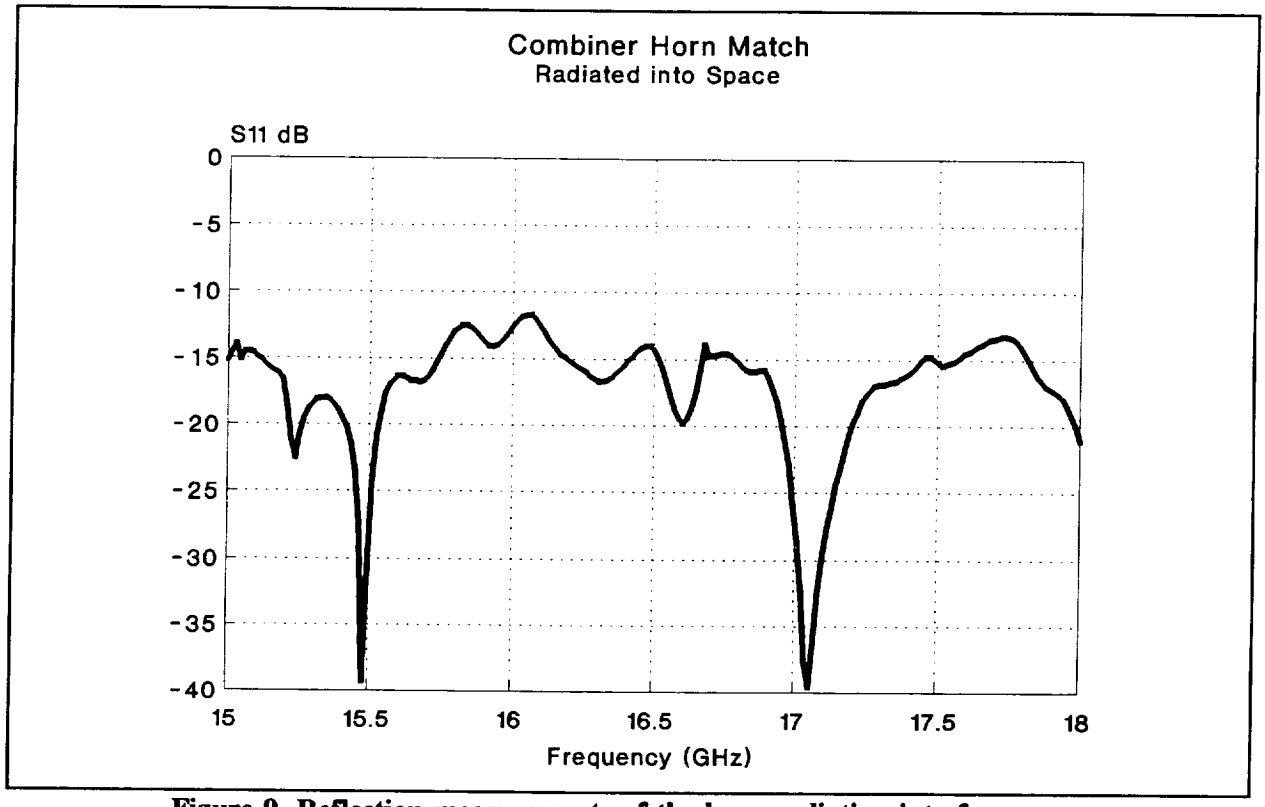

Figure 9 Reflection measurements of the horn radiating into free space

Figure 10 shows the measured 2-way combiner losses of the combiner assembled with the passive feed-through array. The bold line at the top (S21) is the 2-way (round trip) combiner loss in dB. The thin solid and broken lines (S11 and S22, respectively) are the input and output return loss, respectively. The typical two-way combiner loss of the horn was about 6 dB with a 1-dB variation. The minimum loss was 5.0 dB. The return loss was greater than 10 dB over 85 percent of the measured bandwidth from 16.0 to 17.5 GHz and greater than 15 dB over 60 percent of the measured bandwidth.

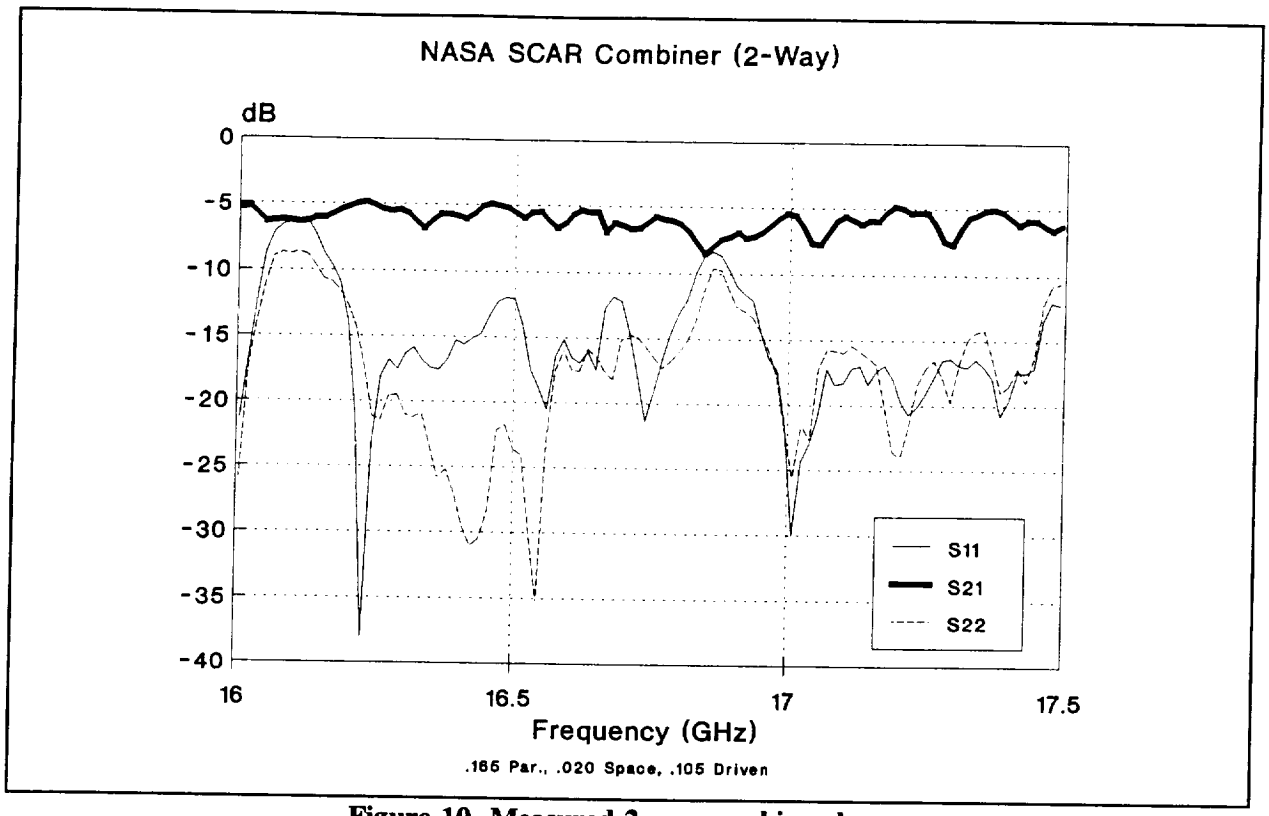

Figure 10 Measured 2-way combiner losses

The insertion loss of the combiner was somewhat higher than originally anticipated. The additional loss was attributed to the dielectric loss of the foam in the slots. To confirm this a test was initiated. The loss of an eight-inch section of Ku-band waveguide filled with the dielectric foam was measured on the network analyzer. The insertion loss was 2.8 dB at 16.5 GHz and 3.0 dB at 18 GHz. This amounts to 0.35 dB per inch. The phase length was also measured. Based on these data, the relative dielectric constant and the loss tangent were calculated as $\epsilon_r=1.332$ and $\tan\delta=0.008$, respectively, at 16.5 GHz. The manufacturer's data sheet shows $\epsilon_r=1.38$ and $\tan\delta=0.006$ at 8.6 GHz.

The loss in the horn due to the dielectric foam was then calculated based on the loss of the foam per unit length (0.35 dB/inch) and the percentage of power in the slots in each section of the horn. The net attenuation was 0.92 dB one-way or 1.84 dB for the round-trip measurement. Hence, a large part of the combiner loss was attributed to the attenuation caused by the relatively high loss tangent ($\tan\delta=0.008$) of the foam. With a perfect dielectric the one-way combiner loss (excluding the microstrip array loss) with the Phase II design would be 1.3 dB to 1.8 dB, based on measured 2-way losses of 5.0 to 6.0 dB. All foam dielectric material is somewhat lossy due to the binder material needed to hold the foam particles together.

A probe of the aperture fields measured on the network analyzer indicated less than 3-dB taper across the aperture in the H-plane. No variation was seen in the E-plane.

Far-field pattern measurements were taken on the NASA SCAR Phase II combiner horn in the E-plane and H-plane at 16, 17, and 18 GHz. The purpose of the test was to determine if uniform field distribution was set up in the aperture of the horn. The measurements were made without the parasitic and driven patch arrays. The 3-piece dielectric lens was inserted in the combiner horn. A plot of the far-field E-plane and H-plane patterns at 17 GHz is shown in Figure 11. Table 4 compares the measured data with theoretical values for two cases: (1) Uniform field distribution and (2) TE_{11}-field distribution of a standard waveguide.

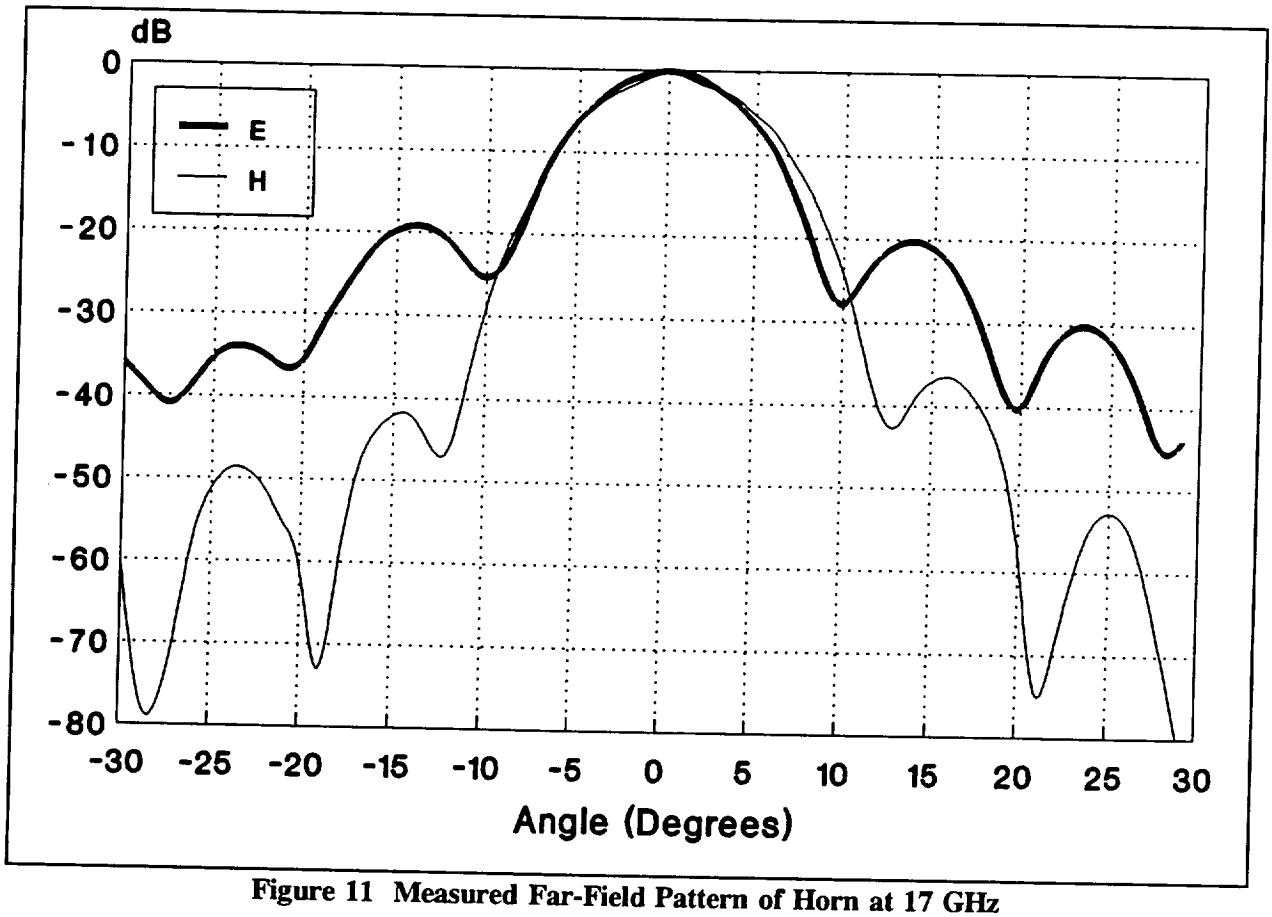

Figure 11 Measured Far-Field Pattern of Horn at 17 GHz

The half power beam width (HPBW) is nearly the same in the E-plane and H-plane at the design frequency of 17 GHz. This matches the condition for near-uniform field distribution. The value of the HPBW is somewhat smaller than the theoretical value, but for good reason. The theoretical value was calculated for a radiated aperture of 4.6 inches in diameter. The pattern measured the

radiation from the entire horn which includes not only the 4.6-inch diameter of the central section, but also the 0.275-inch deep slots around the periphery of the aperture. The slots contain approximately three percent of the total energy.

The level of the first sidelobe of the horn was lower than theoretical values for either uniform field distribution or TE_{11}-mode distribution. However, the influence of the radiated energy from the slots is sufficient to distort the comparison of the measured data of the sidelobes to the theoretical patterns. Compared to a theoretical pattern for uniform field distribution of a 4.6-inch diameter aperture, the pattern for the OSPC should appear to have a narrower HPBW (due to its larger effective diameter) with lower sidelobes (to account for the slight difference in the H-plane taper and tapered power distribution in the slots).

For the reasons presented in the previous paragraph, near-uniform field distribution appears to have been achieved in the Phase II horn. The Phase II horn is closer to having uniform field distribution than it is to having TE_{11}-field distribution and thus represents a significant improvement in this respect over the Phase I horn which had nearly a TE_{11}-mode distribution.

The gain and directivity of the horn was at 25.4 dB and 27.4 dB, respectively. The 2.0 dB difference is the one-way loss as determined from the pattern measurements. This is close to the 2.2 dB loss derived from two-way measurements on the network analyzer.

Table 4 Summary of Far-field Pattern Measurements

Evaluated Parameter	Calculated Uniform Distribution		Measured Horn Data		Calculated TE_{11} Mode Distribution	
	E-PLANE	H-PLANE	E-PLANE	H-PLANE	E-PLANE	H-PLANE
HPBW (Deg.)						
16 GHz	9.4	9.4	**7.0**	**8.3**	9.4	11.9
17 GHz	8.8	8.8	**7.0**	**7.2**	8.8	11.2
18 GHz	8.3	8.3	**6.0**	**7.0**	8.3	10.6
FNBW (Deg)						
16 GHz	22.4	22.4	**22.0**	**27.5**	22.4	31.5
17 GHz	21.1	21.1	**20.0**	**25.0**	21.1	29.6
18 GHz	19.9	19.9	**18.0**	**24.0**	19.9	28.0
FIRST SIDELOBE (dB)			**(Avg**	**2 SL)**		
16 GHz	-17.6	-17.6	**-23.3**	**-36.2**	-17.6	-26.2
17 GHz	-17.6	-17.6	**-19.5**	**-38.2**	-17.6	-26.2
18 GHz	-17.6	-17.6	**-21.5**	**-40.1**	-17.6	-26.2

4.2 Amplifier Circuit

The prototype amplifier was designed using an Avantek MGA 63100 MMIC device. This a two-stage, partially tuned device that allows the user to provide additional input/output matching circuits to tailor the circuit to a desired frequency response. The maximum output power of the device is 22 dBm with 10 volts bias.

The designed amplifier circuit was tested for gain and return loss on the Hewlett Packard 8510B automatic network analyzer. Figure 12 shows the layout and device configuration of a dual amplifier test fixture that was used to characterize the circuit. The amplifier's gain (S21) measured approximately 10 dB as expected, but the output return loss (S22) was only 5 dB. This was not acceptable, so the matching circuit was tuned and a new layout was made. The new circuit improved the output return loss to an acceptable range of 10 to 20 dB. The initial response of the circuit is shown in Figure 13. Figure 14, Figure 15, and Figure 16 show the final response after tuning and redesign for bias voltages of 6.5, 8.5 and 10.0 volts, respectively.

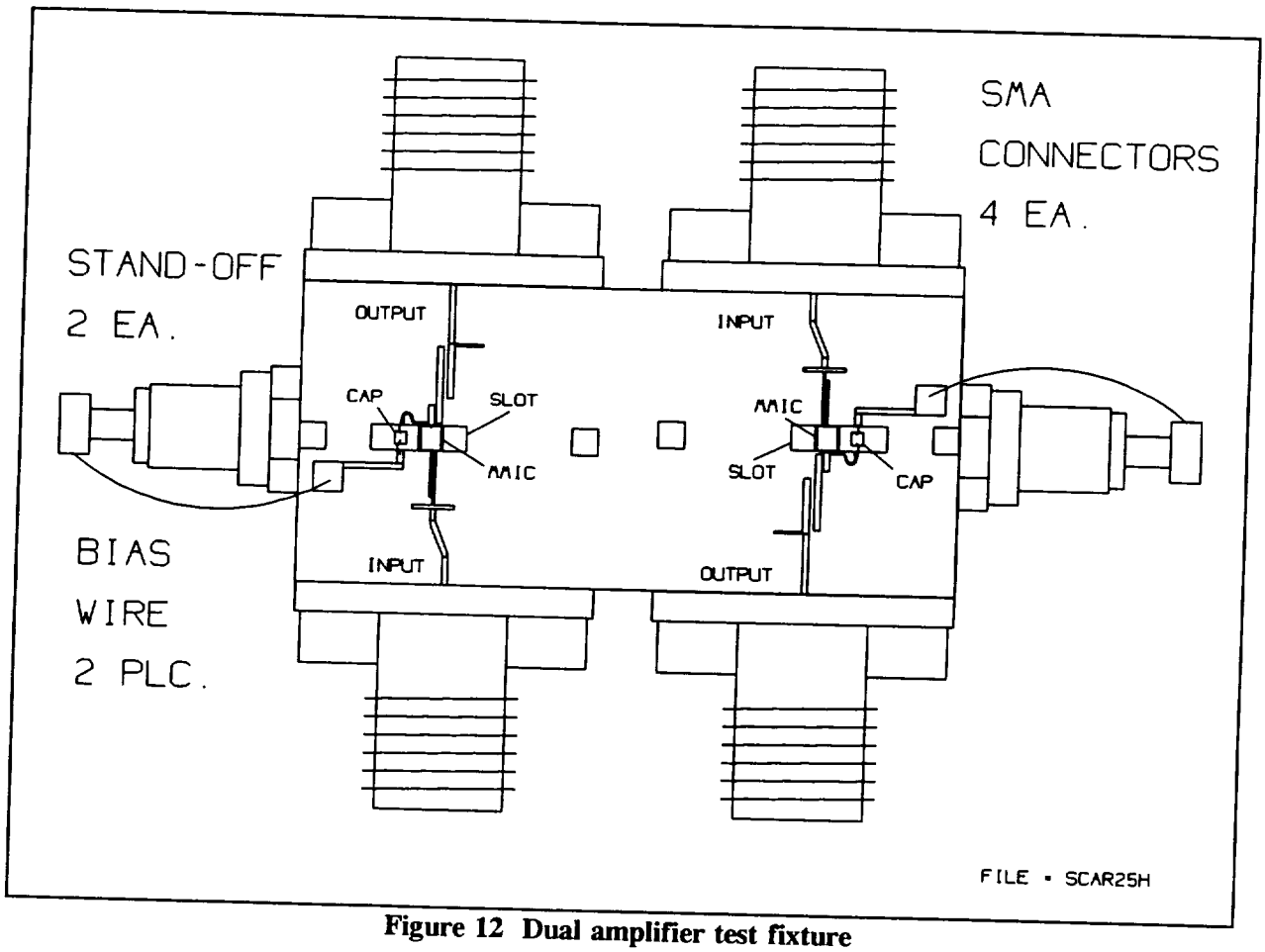

Figure 12 Dual amplifier test fixture

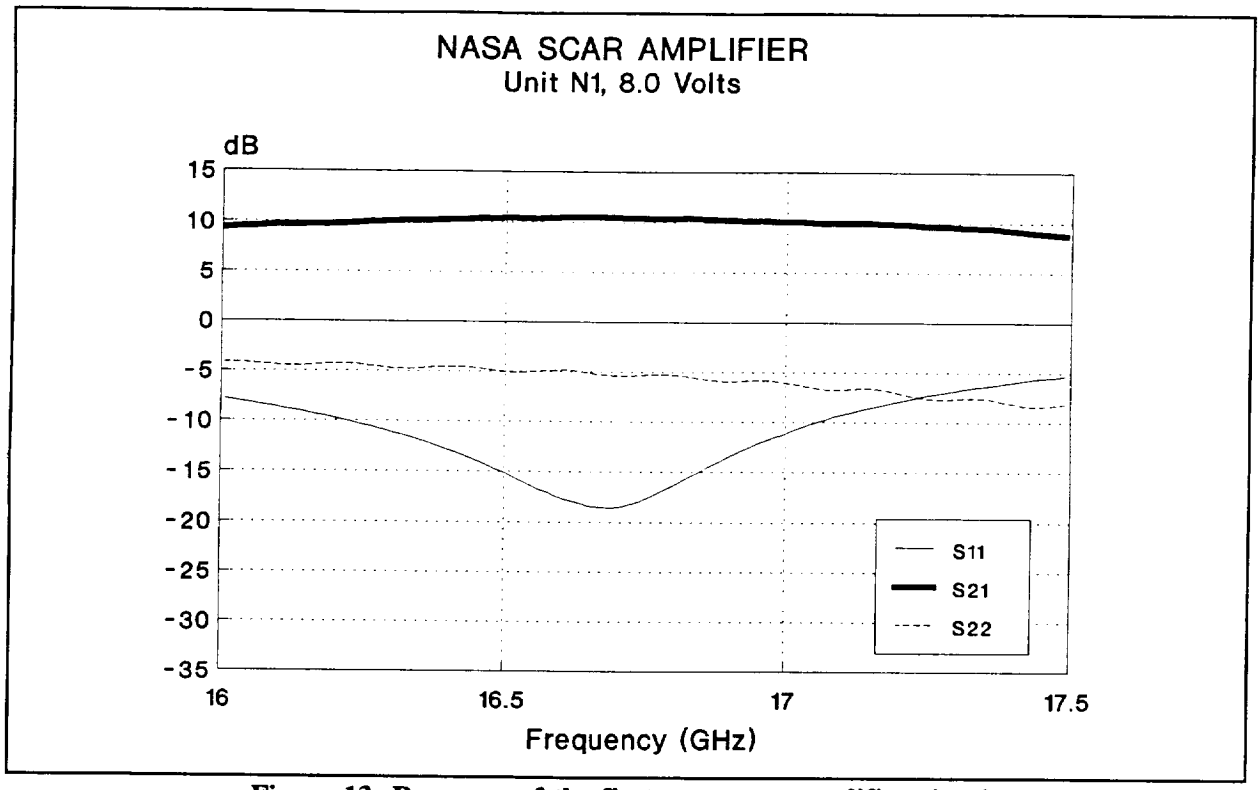

Figure 13 Response of the first prototype amplifier circuit

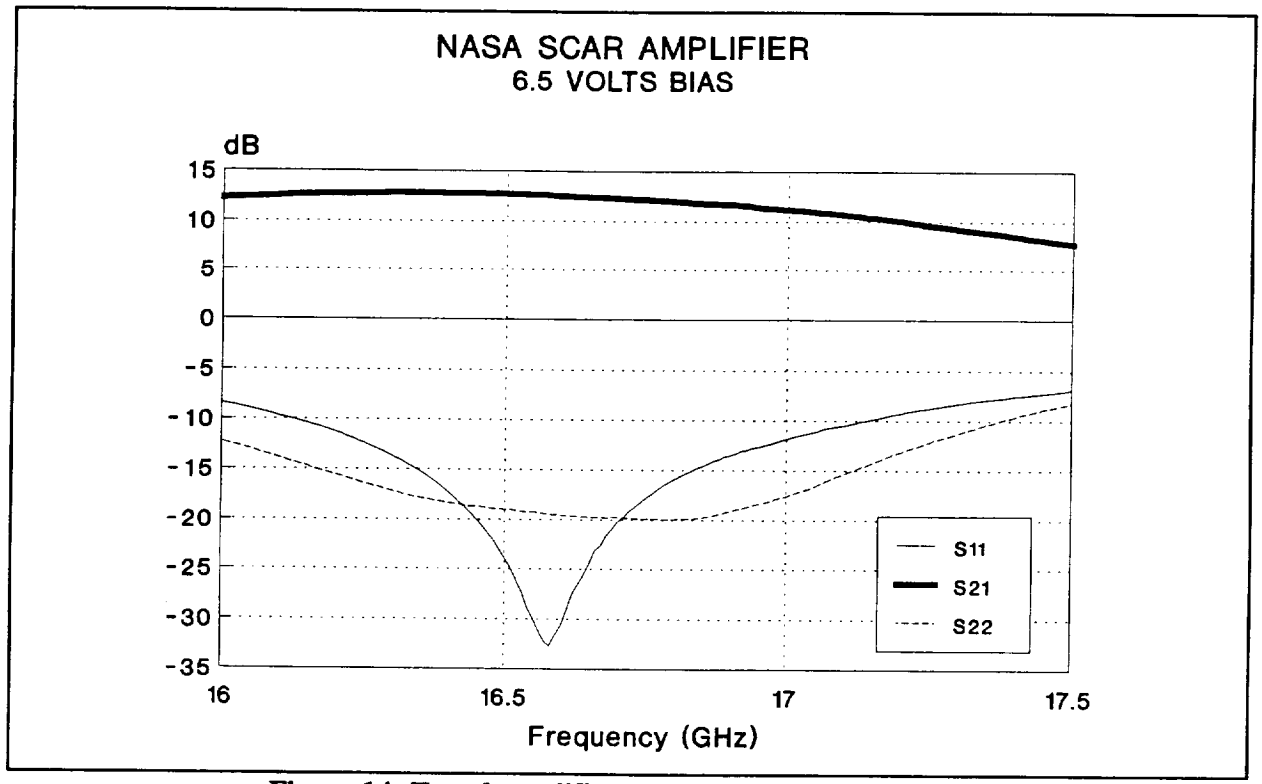

Figure 14 Tuned amplifier response with 6.5 volts bias.

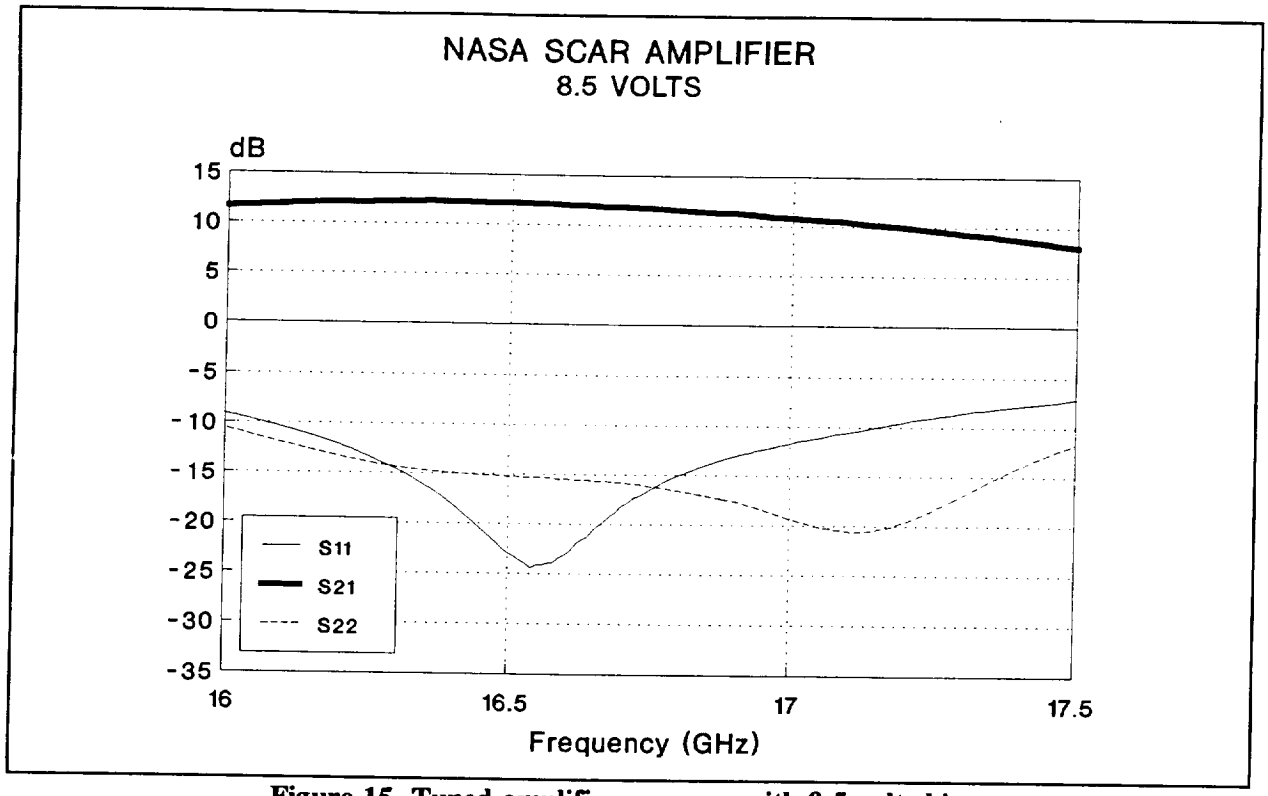

Figure 15 Tuned amplifier response with 8.5 volts bias.

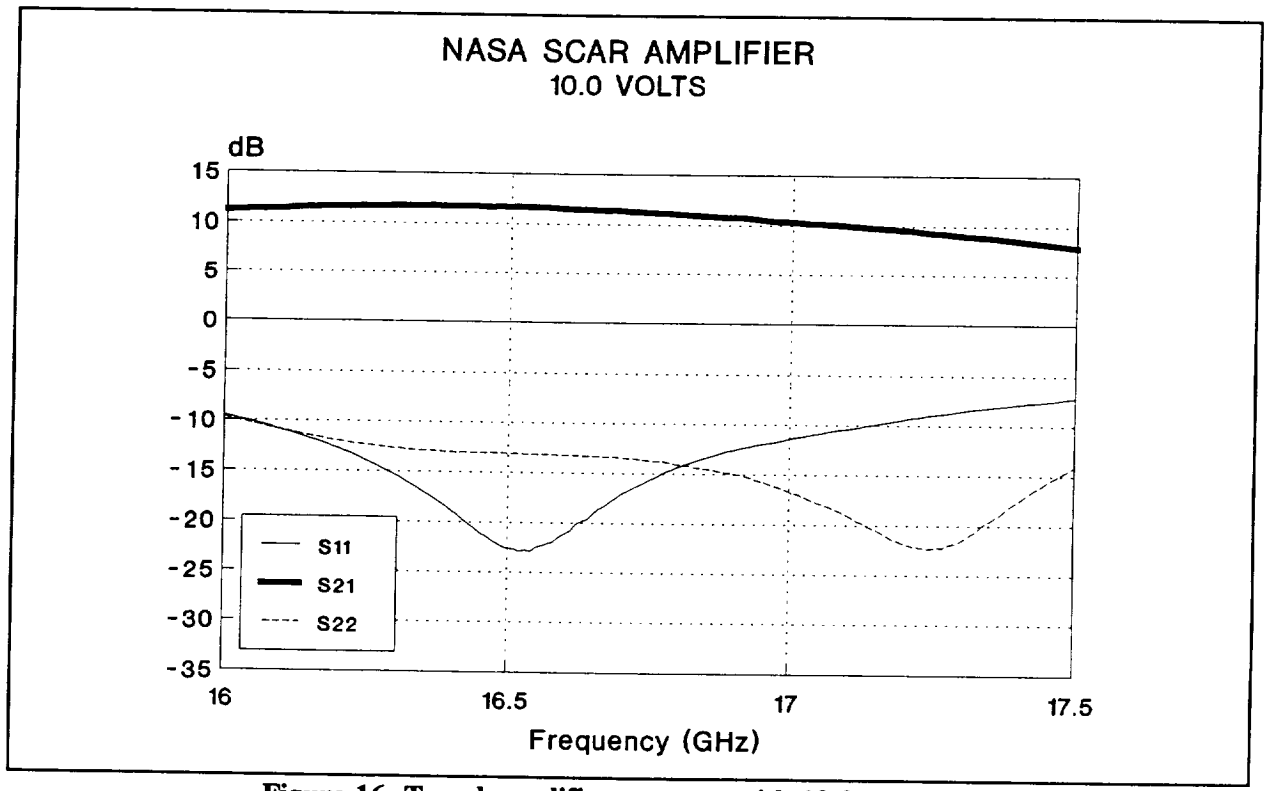

Figure 16 Tuned amplifier response with 10.0 volts bias.

The tuned amplifier circuit was tested as a function of bias voltage and input power. Figure 17 shows a plot of the gain of the circuit as a function of bias voltage for input power levels of -5 and +10 dBm. The measurements were made at 16.4 GHz. The circuit has maximum gain of 13.4 dB for small signals (-5 dBm) at 6.0 volts bias. However, for large input signals (+10.0 dBm), the maximum gain of 11.9 dB occurs at 8.5 volts bias.

Output power is maximized with higher bias voltage. Figure 18 and Figure 19 plot the output power, gain, and efficiency of the amplifier as a function of input power for 6.5 and 8.5 bias voltages, respectively. The amplifier produces higher output power at 8.5 volts than it does at 6.5. Moreover, the linearity is improved considerably. The 1 dB gain compression point occurs at 5.6 dBm input power when biased at 6.5 volts and 9.0 dBm input power when biased at 8.5 volts. Biasing the device at 10 volts would push the 1 dB compression point above 10 dBm input power.

The small signal, (-5 dBm input power), amplifier gain is 1 dB higher when biased at 6.5 volts than when biased at 8.5 volts. However, the large signal, (+10 dBm input power), gain is 0.5 dB higher when biased at 8.5 volts. The power added efficiency is better at the lower bias voltage. The peak efficiency at 11 dBm input power was 13.6% at 6.5 volts and 11.0% at 8.5 volts.

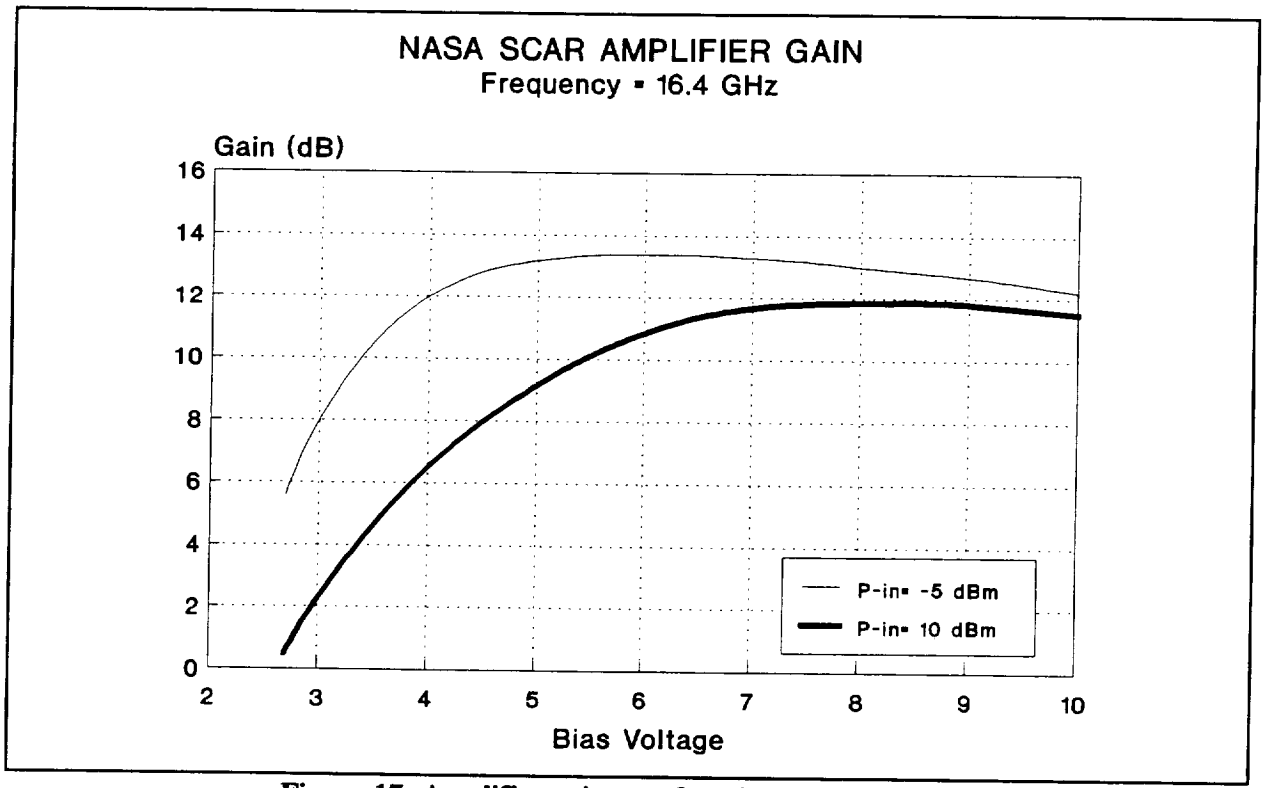

Figure 17 Amplifier gain as a function of bias voltage

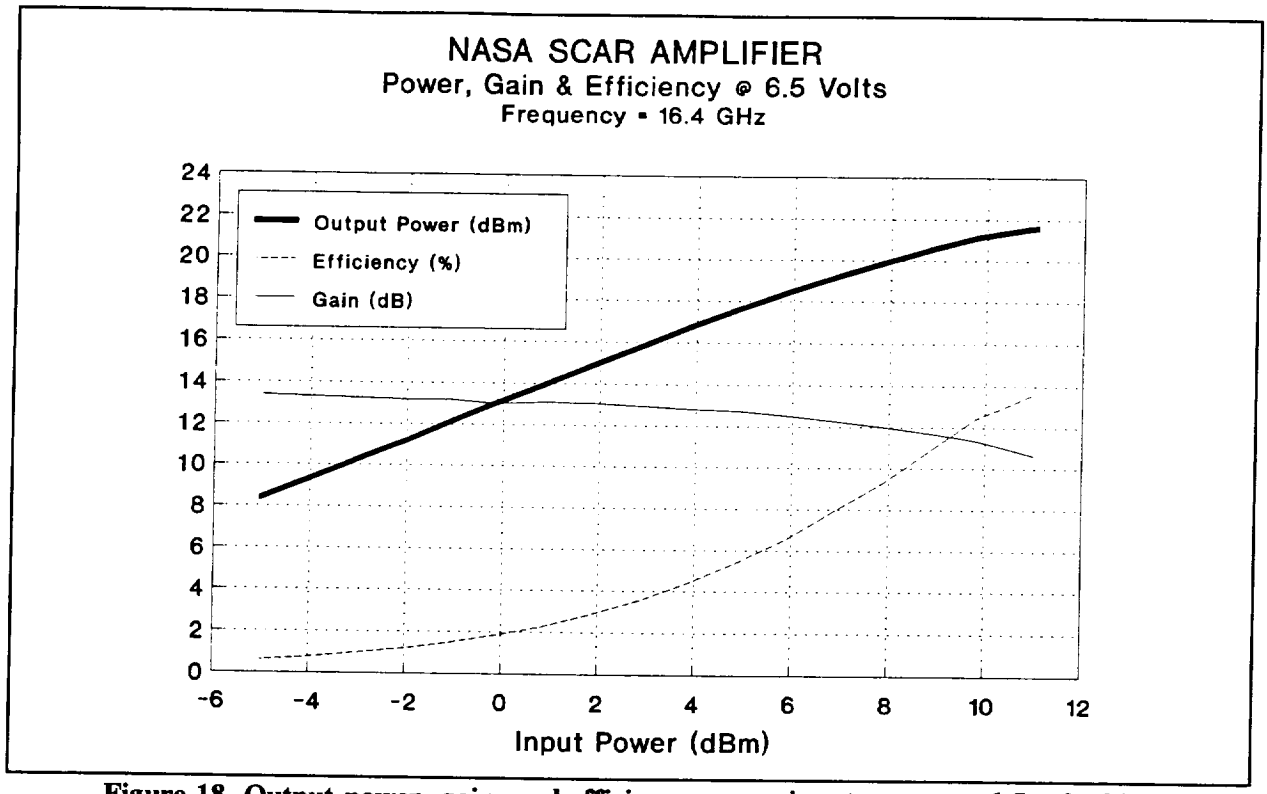

Figure 18 Output power, gain, and efficiency versus input power at 6.5 volts bias

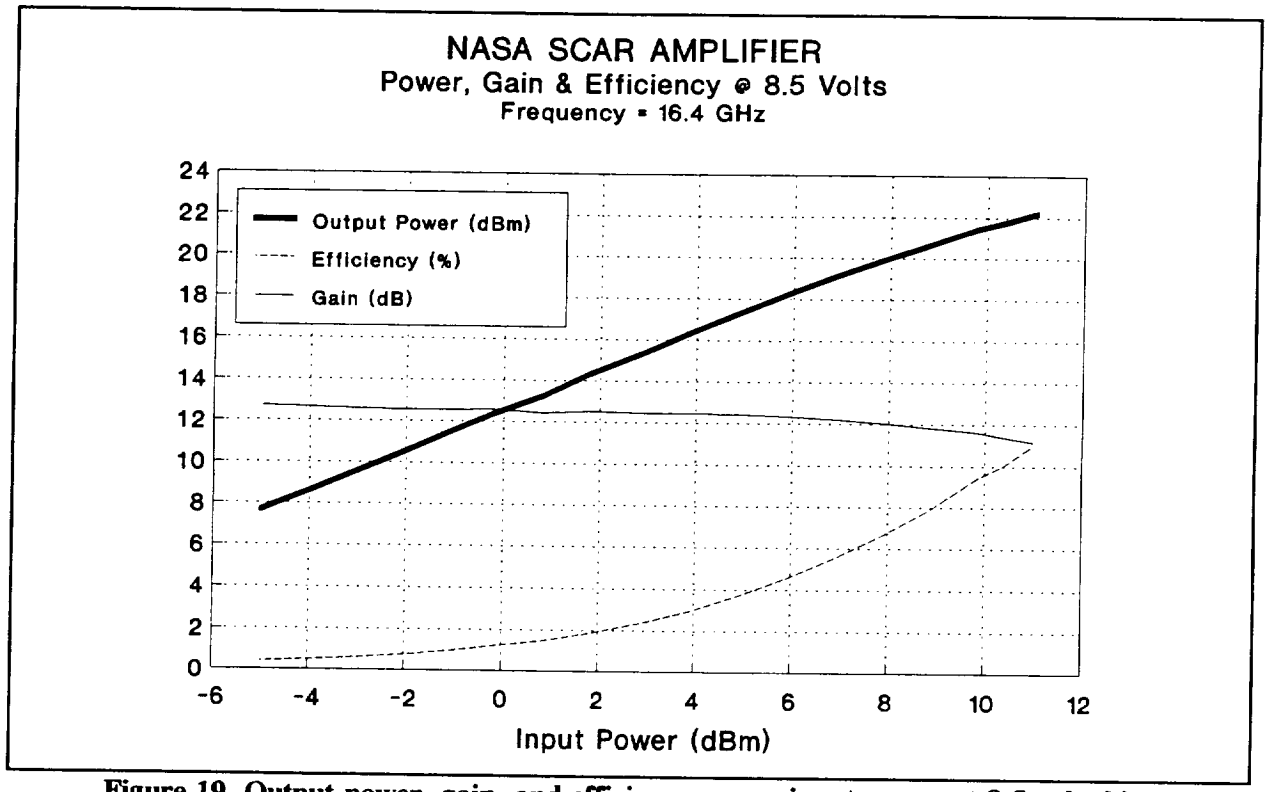

Figure 19 Output power, gain, and efficiency versus input power at 8.5 volts bias

The current drawn by the amplifier circuit varies as a function of voltage. The input power level also has an influence on the amount of current drawn by the amplifier. Figure 20 shows a plot of the amplifier current (in milliamps) as a function of bias voltage for input power levels of -5 dBm and +10 dBm.

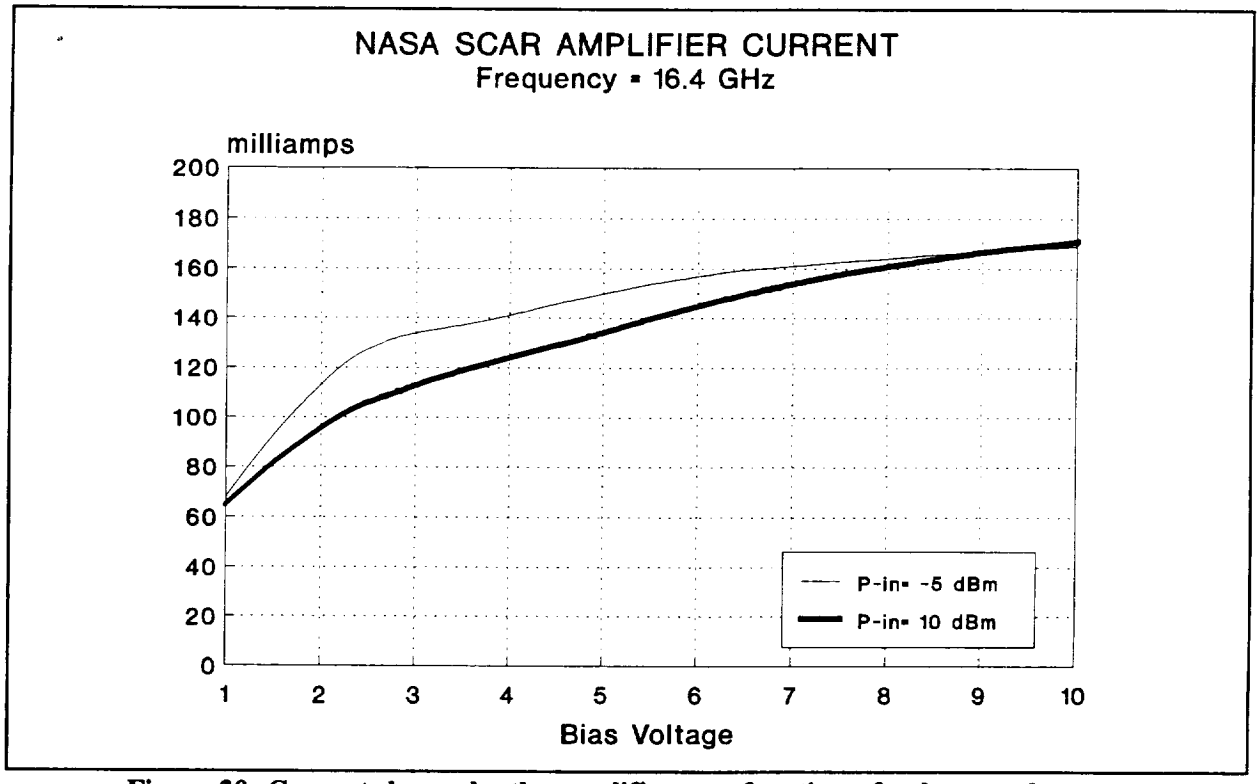

Figure 20 Current drawn by the amplifier as a function of voltage and power

Out-of-band gain of the amplifier circuit was also measured on the network analyzer to confirm that the circuit gain did not exceed the isolation of the orthogonal ports of the patch radiating elements. That isolation exceeds 10 dB from 14 GHz to 20 GHz and exceeds 15 dB from 14.6 GHz to 18.3 GHz. The measured gain of the amplifier is plotted with the port-to-port isolation of the patch radiating element over a broadband frequency range in Figure 21. The difference between the curves is the gain margin for the onset of oscillation due only to the isolation of the orthogonal ports of the patch radiating elements. The plots show a 7.5 dB gain margin.

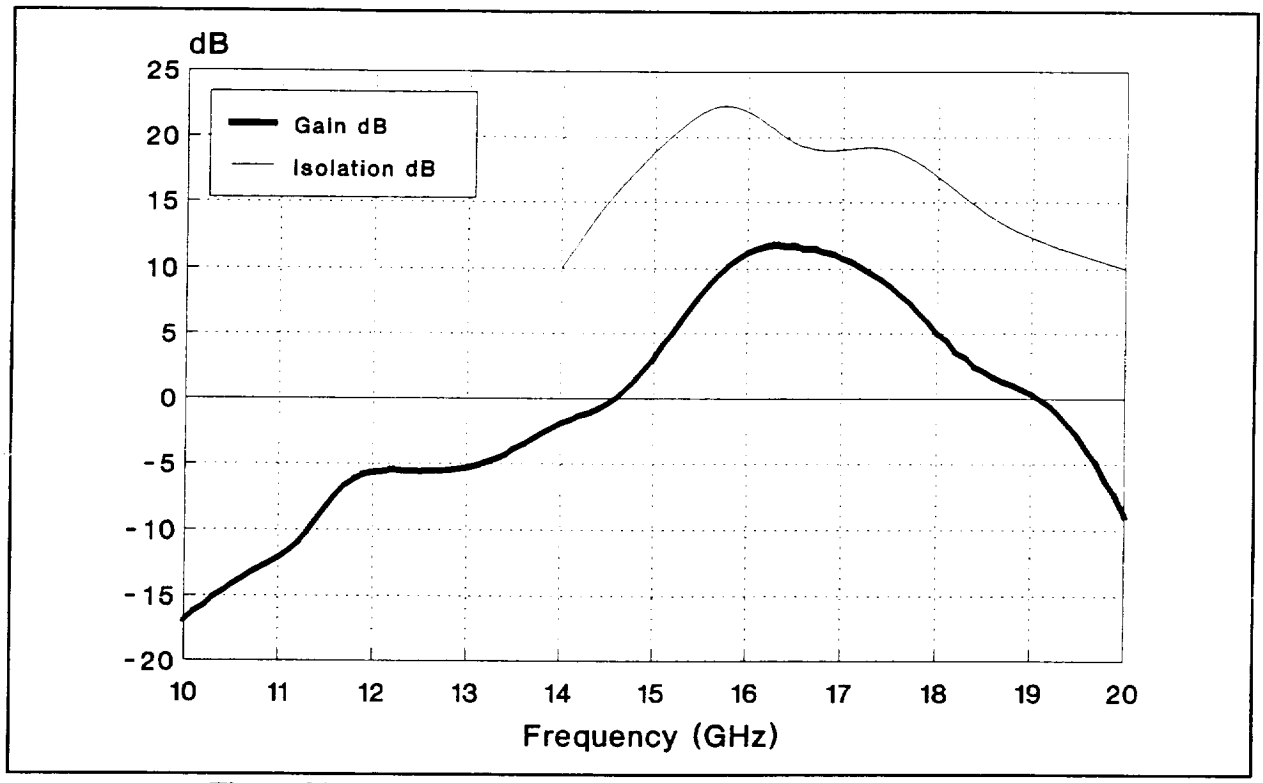

Figure 21 Broadband amplifier gain and patch isolation response

4.3 Amplifier Array

The microstrip layout of the tuned amplifier circuit was duplicated in the array layout. The input and output microstrip lines were routed to the orthogonal ports of the patch radiating elements. Figure 22 shows a diagram of an amplifier circuit element in the array configuration.

The amplifier array was fabricated on a 10-mil thick Duroid™ board that has a dielectric constant of 10.5. The board was metallized with 0.175-mil thick copper on one side. The back side of the board was bonded to a 0.250-inch thick copper plate, which served as a heat sink for the amplifiers.

The array pattern was configured on a 45-degree triangular lattice to match the lattice of the parasitic array and the passive feed-through array. The total diameter of the array board was 7.0 inches; however, the active portion of the array (matching the interior aperture of the horn) was 4.6 inches in diameter.

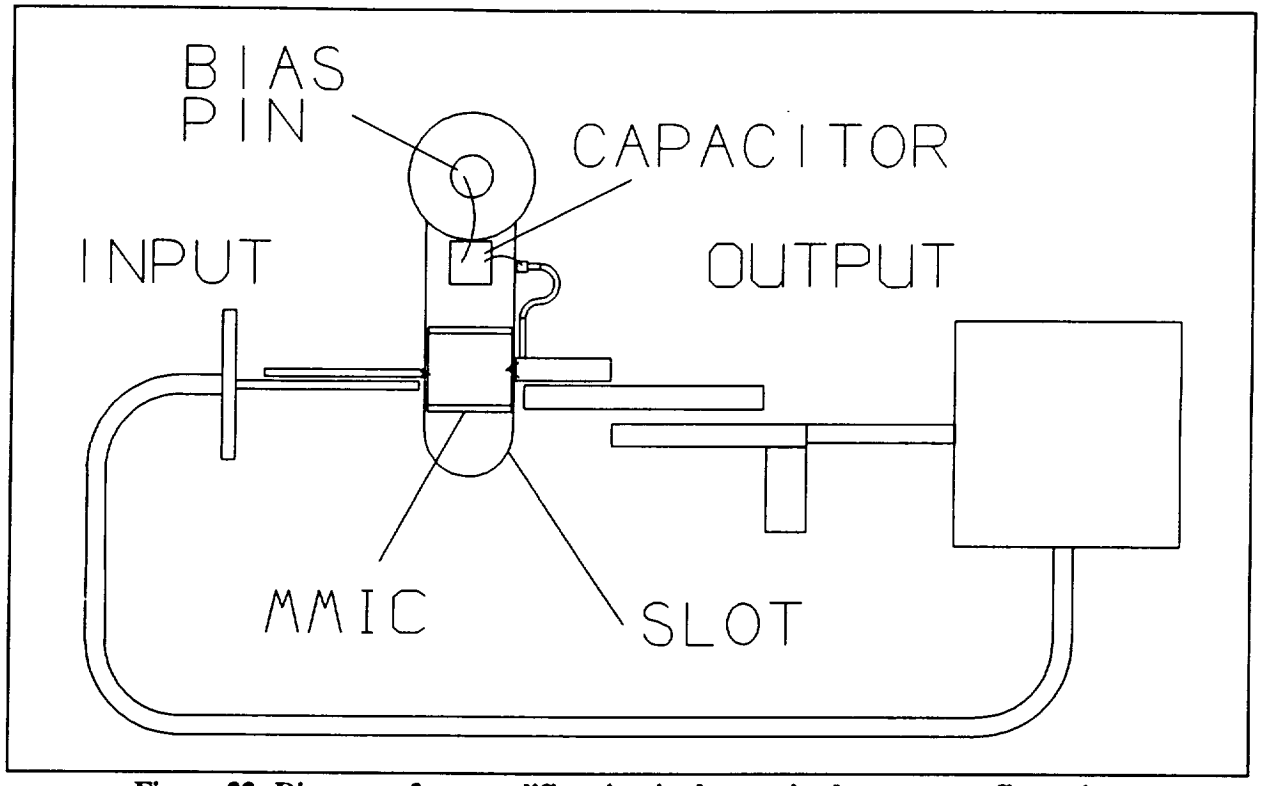

Figure 22 Diagram of an amplifier circuit element in the array configuration

The array board was fabricated in a series of sequential operations. The board was first metallized with a 0.15-mil thick layer of 99.9% gold. The circular array board was then machined out of a 10-inch square board. The pattern was etched using a two-step etching process and a film mask produced from a Gerber file. Sixty-two-mil diameter holes to house the bias pins were drilled through the Duroid™ and the copper plate. The holes were counter-bored on the reverse side to accommodate the 80-mil diameter flange on the bias feed-through pins. Two 62-mil diameter holes were drilled (located by the mask pattern) for location alignment pins. Eight through-holes were drilled on the periphery of the array for the mounting screw holes. The excess Duroid™ material around the periphery was then milled away as the final machining step.

The 69 slots on array board were cut out by hand using an X-acto™ knife and a metal alignment tool. The alignment tool had two dowel pins which located adjacent bias pins holes. By using the slots in the tool, the cut on the Duroid™ board could be accurately controlled achieve required tolerances. Both ends of the bias feed-through pins were cut off to obtain the proper lengths. They were then soldered into the bias pins holes in the array. A 10-mil thick Duroid™ with half-ounce copper cladding on both sides and holes drilled in the bias pin locations was epoxied to the back side of the

array, allowing the bias pins to stick out through the holes. This bias board along with buss wire was used to distribute the applied voltage evenly across the array to all the bias pins.

The MMIC die were soldered to 40-mil square by 5-mil thick Molytabs, which are molybdenum shims. The molytabs served two purposes: (1) They provided height required to bring the top of the 5-mil thick die flush with the height of the 10-mil thick Duroid™, and (2) They provided a thermal expansion interface between the gallium arsenide base of MMIC with the copper plate, relieving thermal-expansion stress on the MMIC chip. The molytabs were epoxied in the slots along with 22-picofarad chip capacitors. The RF input and output pads on MMIC were wire bonded to the corresponding input and output lines on the circuit using 0.7-mil diameter gold wire. The end of the bias line on the circuit was wire bonded to the capacitor and then to the bias pins. See Figure 22 for details of the amplifier element assembly.

Figure 23 shows a photograph of the front view of the completely assembled amplifier array. The back side of the array is shown attached to the Phase II combiner in the photograph in Figure 24.

To determine if each amplifier in the array was working, a special test setup was constructed. An aluminum ring with a 0.5-inch by 0.5-inch thick cross-section was built with tapped holes matching the mounting hole pattern of the array. The array was screwed into the ring and placed on the table, with the radiating patches facing upward. A glass plate was placed on top of the ring. The dual mode port of the orthomode transducer was placed on top of the glass plate and was visually aligned so the dual-mode port of the orthomode transducer was directly above the radiating element. The array was biased on with 8.5 volts and the output port of the transducer was monitored on the spectrum analyzer.

Due to the configuration of the setup, the working amplifier elements oscillated. This was not unexpected, since the parasitic patch array was not in place during this test and both the flange on the orthomode transducer and the glass plate reflected energy back into the radiating elements. The oscillation signals served to indicate whether an individual amplifier was working. If an element was not working, the output signal on the spectrum analyzer would be small or non-existence. In this manner, all elements were checked. Of the 69 elements, five were identified as non-working and subsequently replaced. The method of epoxying the molytabs to the copper plate allowed the devices along with the molytabs to be replaced with little difficulty.

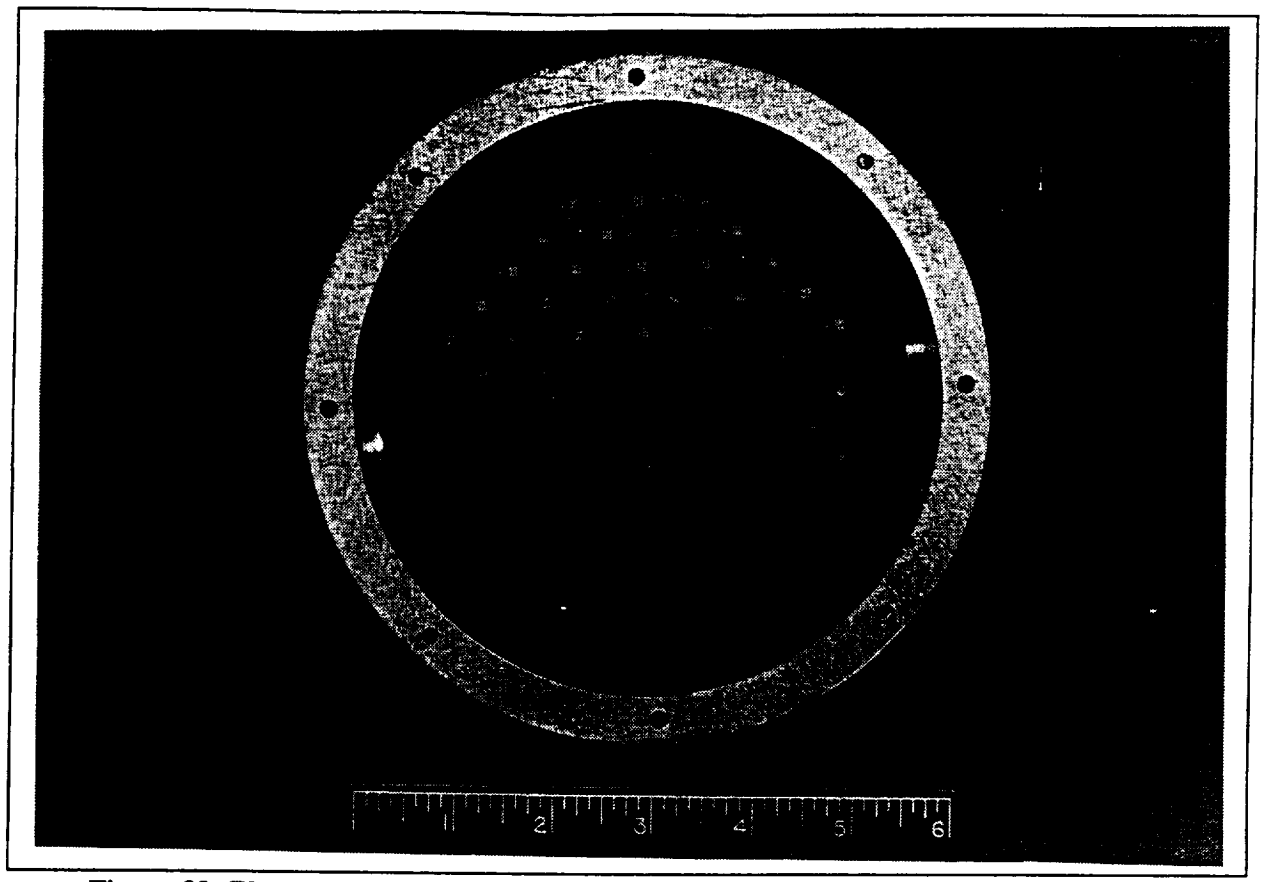

Figure 23 Photograph of the front view of the completely assembled amplifier array

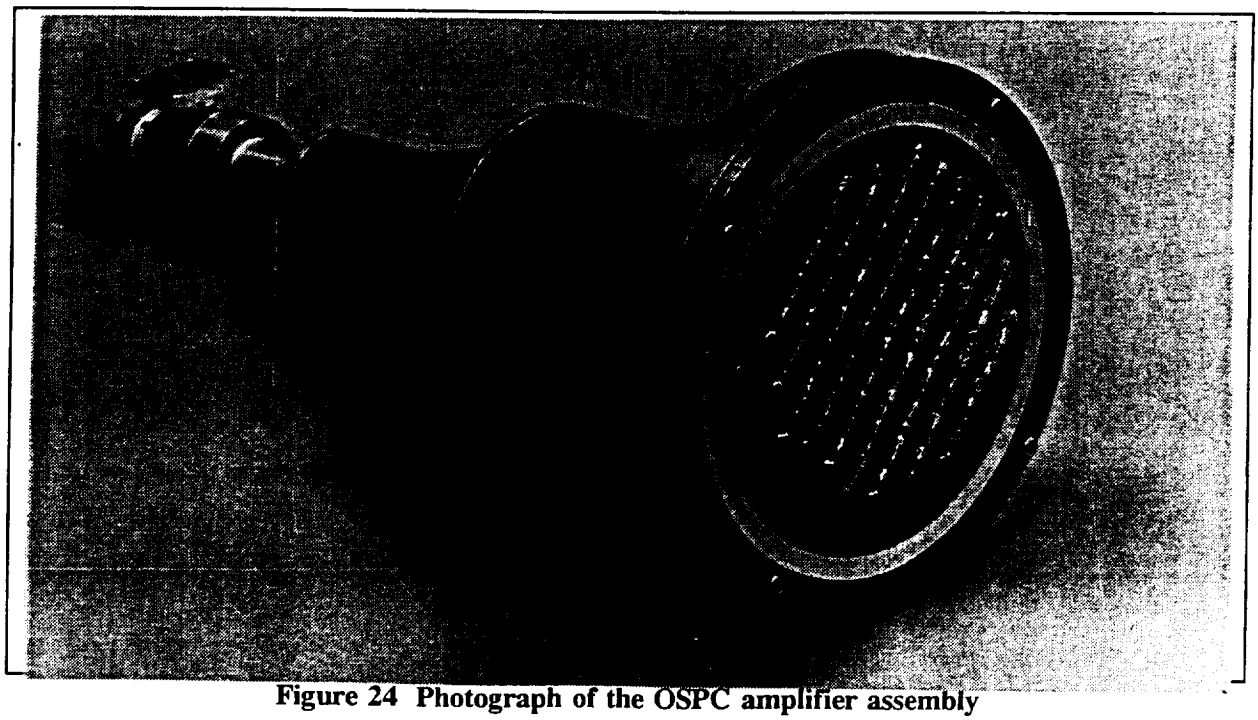

Figure 24 Photograph of the OSPC amplifier assembly

4.4 OSPC Amplifier Tests

The array was assembled to the Phase II combiner and biased on. The output port of the orthomode transducer was connected to a spectrum analyzer to detect any signs of oscillation. The spectrum analyzer revealed that the unit oscillated in-band at 16.4 GHz. The oscillation occurred when the bias to the OSPC amplifiers was raised sufficiently to produce approximately 3-dB gain (based on the measurement of a single-unit, test amplifier). The oscillation was observed when the array was connected to either the Phase I or the Phase II OSPC feedhorns.

No oscillations were observed on the spectrum analyzer when the amplifier array was tested without any enclosing structures other than the last section of the Phase II horn. This one-inch long section was used to hold the parasitic array and the 3-piece dielectric lens in place in front of the array. The orthomode transducer was suspended 10 inches above the center of the array using four rods screwed into a circular plate covered with a microwave absorber. The other ends of the rods were screwed into the last (interface) section of the Phase II horn. The spectrum analyzer was connected to the output port of the orthomode transducer. No oscillations were observed. The 69-element amplifier array was biased at 8.5 volts and 10.5 amperes. No oscillations were observed even when a signal was injected into the input port of the orthomode transducer. The amplitude of the output signal increased as the bias voltage to the array was adjusted from 2 to 8.5 volts, thus indicating array gain. However, the overall amplifier gain (in dB) was negative due to the spillover losses of the horn. (Due to feed spillover losses, only a small portion of the radiated energy from the orthomode transducer was collected by the array. However, the signals that were collected by the array elements were amplified and focused back to the feed.)

Previously, an analysis had been performed to determine the amplification gain required to produce oscillation; this analysis considered four sources of feedback to the amplifiers. The results of this analysis showed a worst case gain margin of 7 dB over the 10-dB amplifier gain. Isolation of the orthogonal fields of the fundamental mode of the horn structure was included as one of the sources in the analysis. However, feedback resulting from the generation of higher-order mode resonances were not included as a contributor in the analysis. Higher-order mode resonances are caused by perturbations in the fields resulting from variations in gain, phase, or power of the amplifier array elements and from unavoidable asymmetry in the OSPC feedhorn.

Since higher-order mode resonances can only exist in a confined structure (one with conducting walls), a free-space feed structure would not support these modes. The observations on the spectrum

analyzer (mentioned previously) support the conclusion that the major source of oscillation was higher-order mode resonances generated within the horn structure. Furthermore, they suggest that a space-fed feedhorn structure would be more suitable than the longitudinally-slotted horn structure developed during the program.

In view of the fact that oscillations occur when the array is connected to the combiner, a plan was developed to evaluate the orthomode spatial power combiner concept without connecting the array to the longitudinally-slotted feedhorns as an amplifier. The three-part test plan is outlined below.

1. Measure the gain of the array on the network analyzer using the passive feed-through array as the reference. To avoid oscillation the array should be configured using the space-fed, orthomode transducer fixture. This will demonstrate the gain of the array.

2. Re-configure the array in the Phase I longitudinally slotted horn configuration and measure the output power of the oscillation signal from the OSPC amplifier. This will show the maximum output power available from the array.

3. Line the Phase I horn with microwave absorber and, by observing the output signals on the spectrum analyzer, determine if oscillation still occurs with the amplifier array biased on. If oscillation does not occur, measure the gain on the network analyzer with both the active and passive arrays. The absence of oscillation would demonstrate that a space-fed lens approach, made by lining the walls with absorbers, has merit. Absorbers on the walls of the horn would attenuate higher-order modes, making the structure appear like a free-space environment.

To perform the first test, the passive feed-through array was installed in the space-fed fixture. The network analyzer was calibrated and a reference measurement was taken on the passive array. The passive array was then replaced with the active array. In the process of turning up the bias voltage to the array, the 12-volt maximum device voltage was exceeded. The transistor devices in the array burned out almost instantaneously due to excessive applied voltage. As a result, no data could be recorded.

Using a Hewlett Packard 6024A power supply, the array had been biased to 8.5 volts on several previous occasions without suffering any detrimental effects. The HP 6024A is a 10-ampere power supply which limits the output current to 10.5 amperes.

On the afternoon of the test, the HP 6024A power supply was replaced with an HP 6274B power supply which has a higher current limit (15 amperes). The power supply was changed to allow the array to be biased at 10 volts without limiting the current to 10.5 amperes. The 10-volt bias level was needed to determine the maximum output power of the array in Test #2. For consistency, the gain test should, therefore, use the same bias level. At 10 volts the 69-element array should draw 11.7 amperes (based on measurements made on a single test amplifier). The individual devices are rated at 12 volts and 0.2 amperes. The amplifier circuits were designed and tested at 10 volts for maximum power operation in accordance with the data sheet supplied by the device manufacturer, Avantek.

In a subsequent investigation, it was determined that the voltage control knob on the HP 6274B power supply is over ten times more sensitive than that of the HP 6024A supply. The 6274B supply requires only one-eighth knob revolution to set the supply to 10 volts, compared with 1.5 revolutions for the 6024A supply. The increased voltage control sensitivity with the 6274B power supply was a contributing factor that led to overshooting the target voltage. Also, current limiting was not set on the HP 6274B power supply at the time of the test.

The damage to the array devices was extensive. Visual examination of the array devices under a microscope revealed that at least 64 of the 69 transistors were burned out.

As a consequence of the array being damaged, the tests outlined in the test plan could not be completed.

4.5 Space-fed Lens Feedhorn Design

A second horn design, using a space-fed lens approach, provides the following potential advantages over the conical horn design: It is a simpler, shorter, and lighter design that provides a means to attenuate any higher-order modes within the horn structure.

Figure 25 shows the cross-sectional view of the space-fed lens design. It consists of a circularly-corrugated horn interfacing with the output of the orthomode transducer. The far-field patterns of the horn illuminate a shaped dielectric lens that has a quarter wavelength impedance matching

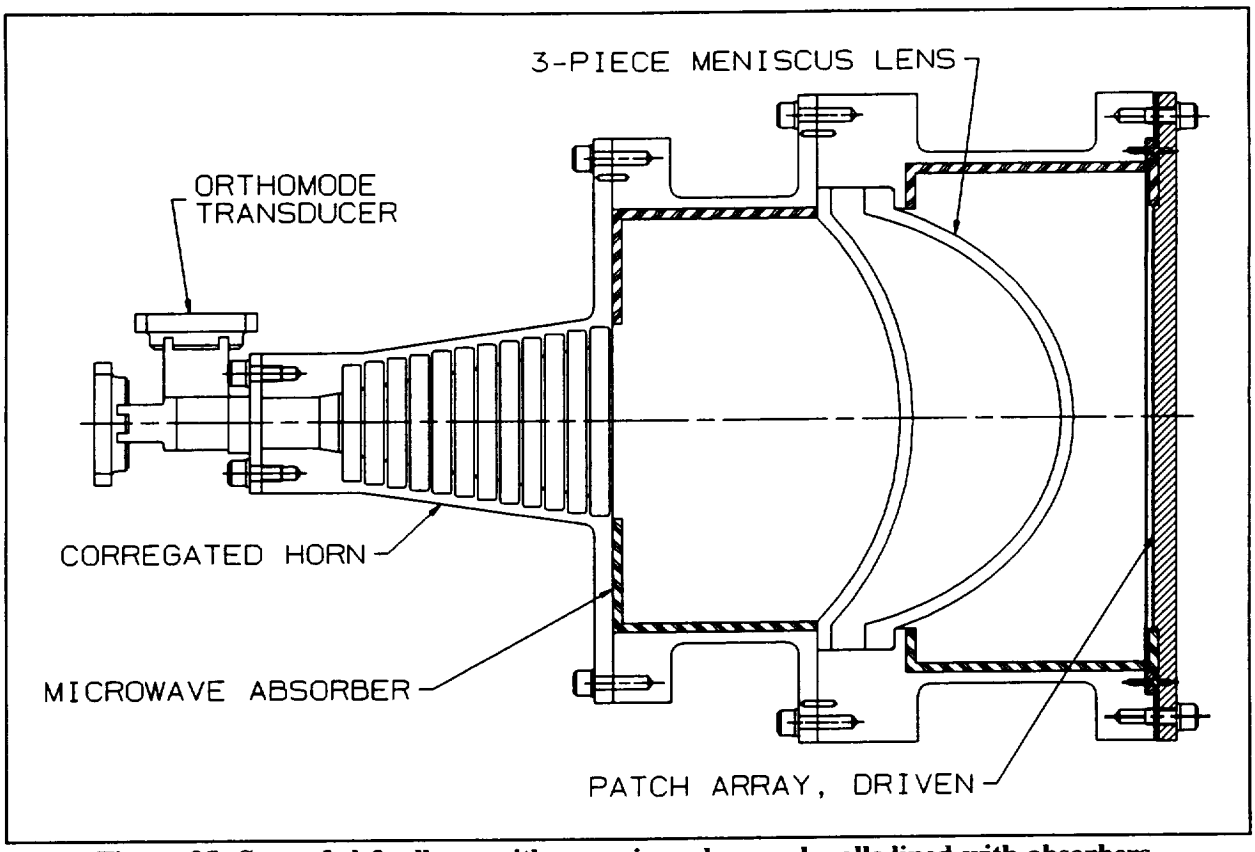

Figure 25 Space-fed feedhorn with a meniscus lens and walls lined with absorbers.

dielectric layer on each lens surface. The shaped lens is designed to produce a uniform field across the exit aperture of the lens. An array of micropatch antenna elements and amplifiers are located at the near field of the shaped lens aperture. Absorbers are bonded to the conductive walls of the horn to damp out any resonances that may occur due to asymmetrical environments and mismatches.

To achieve high performance two key components, the feedhorn and the dielectric lens, must be properly designed. Important requirements for the feedhorn are that it radiates circularly symmetrical patterns and has low sidelobes. A circumferentially corrugated feedhorn satisfies these requirements. An important requirement for the lens is that it transform the feedhorn field pattern to a uniform aperture distribution. Sletten [9] showed that a meniscus lens can satisfy this requirement. A similarly shaped lens design was also analyzed, developed, fabricated, tested and verified at Rockwell in the early 1970's.

Using the computer analysis software developed by Sletten, the feedhorn and the lens physical parameters and electrical performance parameters have been determined and are presented here as a design example. The near-field patterns and physical parameters of the feedhorn were calculated using

Sletten's software, **NEARF.FOR**. The lens physical parameters and electrical performance parameters were calculated by using two programs written by Sletten, **MENISG.BAS** and **LENAMF.BAS**.

The calculated feedhorn spillover loss and edge-taper are listed in Table 5. A typical near-field pattern of the feedhorn is shown in Figure 26. The normalized amplitude distributions at the output aperture of the meniscus lens are shown in Figure 27 for 15.8, 16.75 and 17.6 GHz. As shown, the edge taper on the lens aperture is less than 1 dB over 10 percent bandwidth. The resulting lens shape is shown in Figure 28. Since the lens is symmetrical above its center, only half of the lens aperture is shown. The lens material, Rexolite, has a dielectric constant of 2.54. Estimated combiner losses using the proposed approach are listed in Table 6.

Table 5
Feedhorn Edge Taper and Spillover Loss

Frequency (GHz)	Edge Taper (dB)	Spillover Loss (dB)
15.8	-20.0	0.2
16.75	-21.1	0.2
17.5	-21.5	0.1

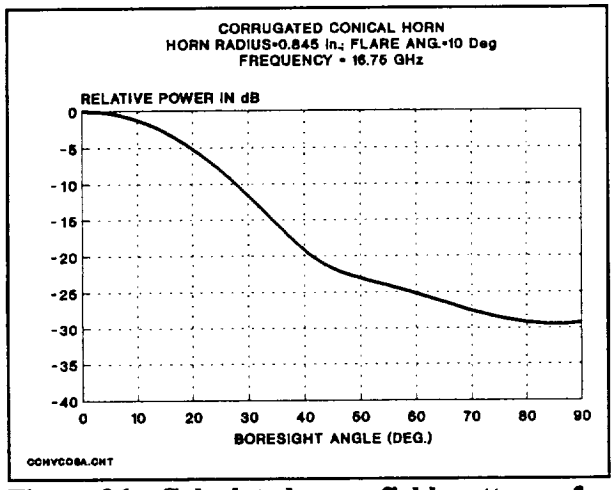

Figure 26 Calculated near field pattern of a circumferentially corrugated horn

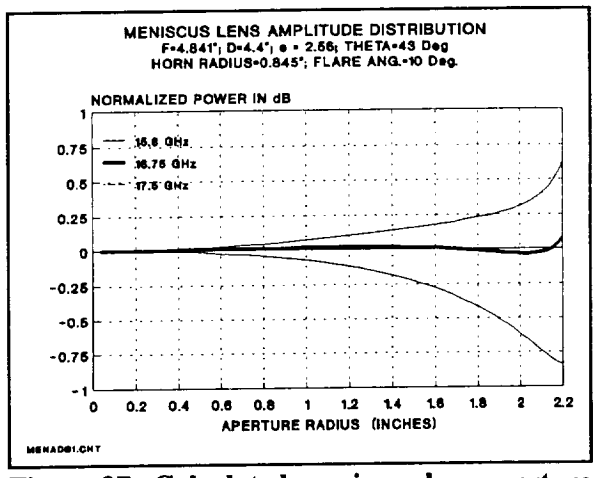

Figure 27 Calculated meniscus lens aperture distribution at 15.8, 16.75 and 17.6 GHz.

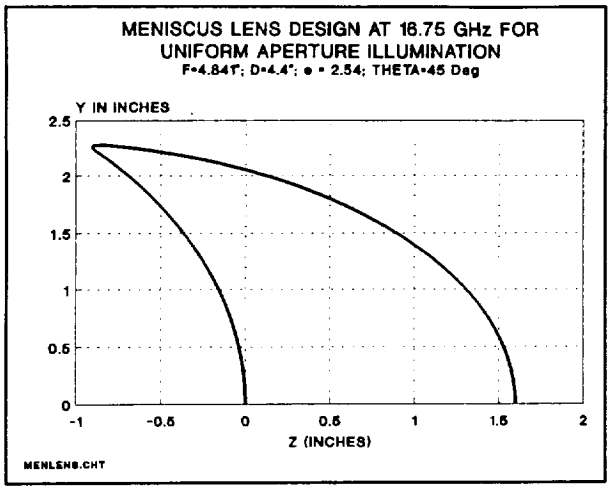

Figure 28 Shape contour of a 4.4-inch diameter meniscus lens

Table 6 Estimated Combiner Losses for Space-Fed Lens Feedhorn Design

Source	Loss (dB)
Mismatch	0.50
Feed Pattern Spillover	0.25
Dielectric Lens	0.25
Horn Conductor	0.25
TOTAL	**1.25**

5.0 RECOMMENDATIONS FOR IMPROVEMENTS

The test results of the OSPC amplifier demonstrate the need to minimize all sources of feedback that could cause oscillation. In an orthomode spatial power combiner the gain of the amplifier elements may not exceed the magnitude of the sum of all sources of feedback. Oscillation will occur if this principle is violated. This factor is difficult to determine since not all sources of feedback can be calculated readily. Therefore, sources of feedback from all sources must be minimized. Improvements can be made to both the feedhorn and array design to eliminate or significantly reduce feedback to amplifier elements.

5.1 Feedhorn Design

The feedback analysis showed that the OSPC amplifier had 7 dB of gain margin before the onset of oscillation. However, the test results did not bear that out. The reason for this is that the analysis did not include the presence of higher-order mode resonances in the horn structure. These higher-order mode resonances are a major feedback contributor to the generation of oscillation.

The use of any closed walled feedhorn for the OSPC will likely produce oscillations in the amplifier. It is statistically improbable to have perfectly symmetric fields within the horn structure or in the amplifier array. All transistor devices, even those produced in the same lot, have some amount of variation. Hence, the gain, output power, and phase length of the devices will vary. Likewise, a

feedhorn will have some amount of variation in symmetry. These variations will generate higher-order mode resonances. If the horn structure does not attenuate these modes, they will propagate back to the amplifier array and cause oscillations within the amplifier. The ideal spatial power combiner amplifier should be able to amplify without oscillations in spite of variations in or even failures of individual amplifier elements within the array.

The space-fed, meniscus feedhorn approach will most likely provide the solution to the feedhorn problem. Higher-order waveguide mode resonances can only exist in a structure enclosed by conducting walls. The space-fed horn uses microwave absorber material on the walls to simulate a free-space environment, in which waveguide mode resonances cannot exist.

5.2 Array Design

Further improvement in the reduction of feedback can be obtained by modifying the array design. As depicted previously in Figure 22, the amplifier array elements in the present design have large microstrip loops from the input port of the radiating element to its output port. Fields surrounding the microstrip lines are weakly coupled to near-by loops. Furthermore, the loop may radiate or receive radiated energy from the feedhorn. Eliminating the loops would reduce the likelihood of significant feedback.

Figure 29 shows an array layout which reduces undesirable radiation and coupling that produce feedback. The amplifier circuit obtains its input signal from one radiating patch element and sends its output signal to another patch. This array layout offers improvements in four areas: (1) It eliminates the large microstrip line loop which could act as a radiating source; (2) It eliminates three bent microstrip lines which also radiate; (3) It provides greater separation between the lines, thereby reducing coupling; and (4) It shortens the total microstrip path length, thereby reducing both coupling and insertion loss.

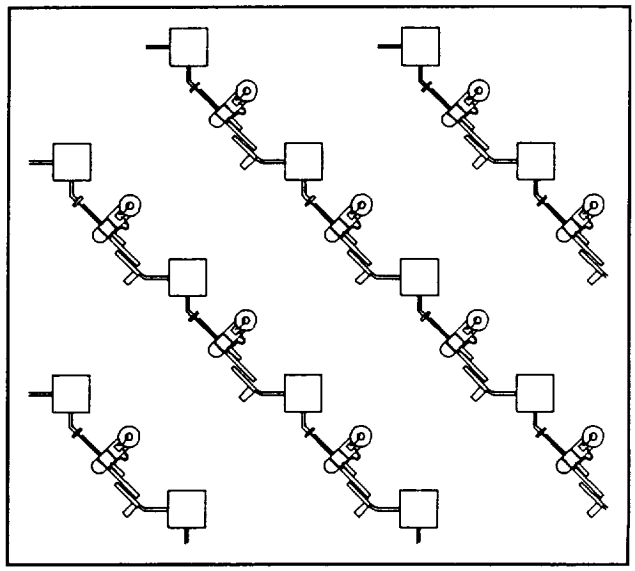

Figure 29 Alternate array layout designed to reduce feedback

6.0 CONCLUSIONS

Key components that are both important and necessary for the OSPC amplifier to function were developed and their performances verified. The 69-element MMIC amplifier array was fabricated, and, using a space-fed horn, small-signal amplification gain from the array was observed on a spectrum analyzer. No oscillations were observed on the spectrum analyzer even when RF power was injected to the array with the array biased at 8.5 volts, corresponding to at least 10-dB gain.

The objective of the Phase II NASA SCAR effort has been to demonstrate high-power amplification using an orthomode spatial power combiner (OSPC) to combine RF output from a two-dimensional array of amplifiers. Since the OSPC amplifier designed and developed to achieve this objective exhibited oscillations induced by higher-order mode resonances, the stated design goals for this effort were not adequately achieved. The OSPC did not achieve its objective for two reasons: (1) The dielectric loss of the foam in the longitudinal slots was too high, resulting in over 5 dB (two-way) insertion loss, and (2) The longitudinally-slotted horn provided no means to attenuate high-order mode resonances developed as a result of field variations in the aperture.

The causes of the problems with the combiner were identified. A different horn, using a space-fed lens approach, was designed but not fabricated. This design approach shows potential for eliminating the causes of oscillation obtained with the longitudinally slotted horn combiner. Higher-order waveguide mode resonances can only exist in a structure enclosed by conducting walls. The space-fed horn uses microwave absorber material on the walls to simulate a free-space environment, which is free of waveguide modes.

The efforts put forth under Phase II of the NASA SCAR program have contributed to the technology of spatial power combining in several ways. (1) They have demonstrated that the orthogonal mode concept will not work in a closed walled structure because reflections from higher-order mode resonances generated by field perturbations will cause oscillations. (2) They have shown that a space-fed approach without enclosing walls can capture amplified signals from an array with orthogonally-polarized input and output signals. (3) They have led to the design of a space-fed lens feedhorn which has the potential to achieve high efficiency spatial power combining from a two-dimensional array of amplifiers. The work performed on this project has served to further the pursuit of spatial power combining technology by (1) providing insight into the sources of and solutions to practical limitations of one approach and (2) pointing out an alternate approach with apparent potential for future applications.

7.0 REFERENCES

1. "NASA SCAR Program First Quarterly Status Report," dated 14 January 1991.

2. "NASA SCAR Program Second Quarterly Status Report," dated 12 April 1991.

3. "NASA SCAR Program Phase I Final Report," dated 27 February 1992.

4. "NASA SCAR Phase II First Quarterly Status Report," dated 17 September 1992.

5. "NASA SCAR Phase II Second Quarterly Status Report," dated 18 December 1992.

6. "NASA SCAR Phase II Third Quarterly Status Report," dated 25 March 1993.

7. Scharten, T., Nellen, J., and Van de Bogart, F., "Longitudinally Slotted Conical Horn Antenna With Small Flare Angle", ***IEEE Proceedings***, Vol. 128, pt, H, No. 3, June 1981; pp 117-123.

8. Aly, M. S. and Mahmoud, S. F., "Propagation and Radiation Behavior of a Longitudinally Slotted Horn With Dielectrically Filled Slots", ***IEEE Proceedings***, Vol. 132, Pt. H, No. 7, December 1985; pp 477-479.

9. Sletten, C. J. (editor), ***Reflector and Lens Antennas: Analysis and Design Using PC's***, Version 2.0, Artech House, Norwood, MA, 1991.